2017-03-01

A Quaternary climate record from a Uinta Mountains, USA, fen core with emphasis on sediment pyrolysis

Samuel Abraham Hillam
Brigham Young University

A Quaternary Climate Record from a Uinta Mountains, USA, Fen Core with Emphasis on Sediment Pyrolysis

Samuel Abraham Hillam

A thesis submitted to the faculty of
Brigham Young University
in partial fulfillment of the requirements for the degree of

Master of Science

Steve Nelson, Chair
Sam Hudson
Greg Carling

Department of Geological Sciences

Brigham Young University

ABSTRACT

A Quaternary Climate Record from a Uinta Mountains, USA, Fen Core
with Emphasis on Sediment Pyrolysis

Samuel Abraham Hillam
Department of Geological Sciences, BYU
Master of Science

The northern slopes of the Uinta Mountains, Utah were previously glaciated and contain many landslides. The Tokewanna Landslide is very large and lacks Quaternary faults. Presumably, increased moisture was the failure trigger. A Quaternary climate record from a cored fen, developed in a small basin between hummocks, was reconstructed using sediment pyrolysis, biomass balance, and magnetic susceptibility. Pyrolysis is used to define Hydrogen Indices that are used to delineate wetter and drier conditions based on the kerogen type - Type III being drier, and Type II wetter. The data were matched to a time/depth curve and compared to other Uinta Mountains climate studies. Pyrolysis, biomass balance, and magnetic susceptibility results indicate drier to wetter conditions from ~11,027 to ~8,800 cal yr BP. This was followed by an increase in precipitation, peaking ~8,060 cal yr BP, and then decreasing. Drying conditions ensued after ~4,800 cal yr BP, and from ~1,700 cal yr BP to modern. Regional studies suggest mid-Holocene Epoch warming; some also indicate increased precipitation during those periods. A study at nearby Little Lyman Lake (Tingstad et al., 2011) displays a plankton percent record similar to the wetness record of the study fen. The fen core record does not indicate wet conditions at its base as expected. The record begins ~11,000 cal yr BP and likely represents an incomplete history of this Holocene fen, as the base of the wetland deposits was not reached.

Keywords: Uinta Mountains, modern sediments, pyrolysis, Holocene, wetland, fen, paleoclimate

ACKNOWLEDGEMENTS

I want to thank all of those who have loved and supported me through this research and time of study. My wonderful wife, Melissa, has been a source of unending strength, support, and care through this process. Her undeserved love provided great strength.

Steve Nelson, my chair and mentor, has also supported me in ways I could not have imagined when I started. His leadership, curiosity, generosity, and scientific knowledge were all coupled with an immense desire for me to succeed. He seemed to always be able to find an answer to each new problem I believed was going to nullify all my effort. He was also a huge help with ArcGIS and other software applications. It was his funding that provided the means to complete this research as well. Thank you Steve.

Along with Steve, I want to thank my committee members, Sam Hudson and Greg Carling. The use of their equipment and labs, as well as procedural direction helped me obtain much of my data. Their flexibility allowed me to try and retry until usable data was generated.

I also want to thank those that helped with the rest of my lab and field work. Kevin Rey and Dave Tingey contributed significant training, oversight, and sample processing help. Thank you to J. C. Tucker as well for sample preparation help.

Lastly, I want to thank my family members. I know many prayers have been offered on my behalf and I have felt them being answered. My sister Alane helped me with Adobe Illustrator, taking it from an intimidating mystery to a useful tool. Thank you all.

TABLE OF CONTENTS

LIST OF FIGURES

Introduction

The Uinta Mountains are an east-west trending mountain range of Laramide age ~ 50-70 M. They are in northeastern Utah directly below the Utah - Wyoming border and extend approximately 200 km in length (Fig. 1) (Corbett and Munroe, 2010). The core of the mountains was originally formed as a neo-Proterozoic sedimentary basin. It uplifted as a cohesive block of quartzite, slate, and shale to form an anticline during Laramide thrusting (Hansen, 2005; Louderback et al., 2014). Younger sequences of rocks atop the PreCambrian strata include shales and the Bishop Conglomerate (Hansen, 2005).

The Bishop Conglomerate is observed to be as thick as 182 meters and consists of an upper and lower unit. The upper unit contains more friable, pebbly sandstone, tuffaceous sandstone, and tuff; whereas the lower unit is mostly moderately well cemented boulder and cobble size conglomerate (Hansen, 1984; Kowallis and Bradfield, 2005; Kowallis et al., 2005). The Bishop Conglomerate is primarily quartzite from the Uinta Mountain Group that eroded during Cenozioc time uplift (Untermann and Untermann, 1969).

Slope failure involving the Bishop Conglomerate is not uncommon (Bradfield, 2007). As the permeable conglomerate becomes water saturated it becomes heavy and adds stress to weaker underlying formations. The weaker substrata act as the slip plane for many landslides along the slopes of the Uinta Mountains (Bradfield, 2007). One such landslide is on the northern slope on the eastern side of the Blacks Fork River drainage, herein called the Tokewanna

landslide. The slide is far from any Quaternary faulting, indicating slope failure must have been caused by another factor, such as wetter conditions. To understand the climate variance since the slide, a fen constructed on its surface was percussion cored proxy studies.

Previous climate proxy studies in the Uinta Mountains have been explored. Munroe (2003) utilized historical rephotography of the northern Uinta Range to observe vegetation responses to modern climate warming; Corbett and Munroe (2010) used lake sediment cores to examine loss on ignition, sediment grain size, C/N ratios, and biogenic silica to construct a Quaternary climate response of two lakes; Munroe and Mickelson (2002) reconstructed mean glacial equilibrium lines using accumulation-area ratio, toe-headwall altitude ratio, highest elevation of continuous lateral moraines, and cirque-floor elevations; Tingstad et al. (2011) documented lake core diatom assemblages to interpret climate change over the past 13,000 years; Koll (2012) and Louderback et al. (2015) analyzed pollen and charcoal records from Holocene aged cores.

The objective of this study is to identify vegetation changes from a fen on the Tokewanna slide, referred to here as the Tokewanna fen, that can be correlated to wet and dry conditions to understand climate change since the slide movement. The proxies used are sediment pyrolysis, biomass balance, and magnetic susceptibility. Pyrolysis can be used to classify the kerogen types, which can be attributed to wetter or drier conditions based on geochemical differences in organic matter derived from algae versus vascular terrestrial plants. Increased biomass suggests

increased vegetation, and thereby moisture, and magnetic susceptibility spikes can indicate drier climates with increased windblown dust or greater influxes of water-borne mineral sediment. In concert, these proxies can help create a climate history for the Tokewanna fen that can be compared to other regional studies.

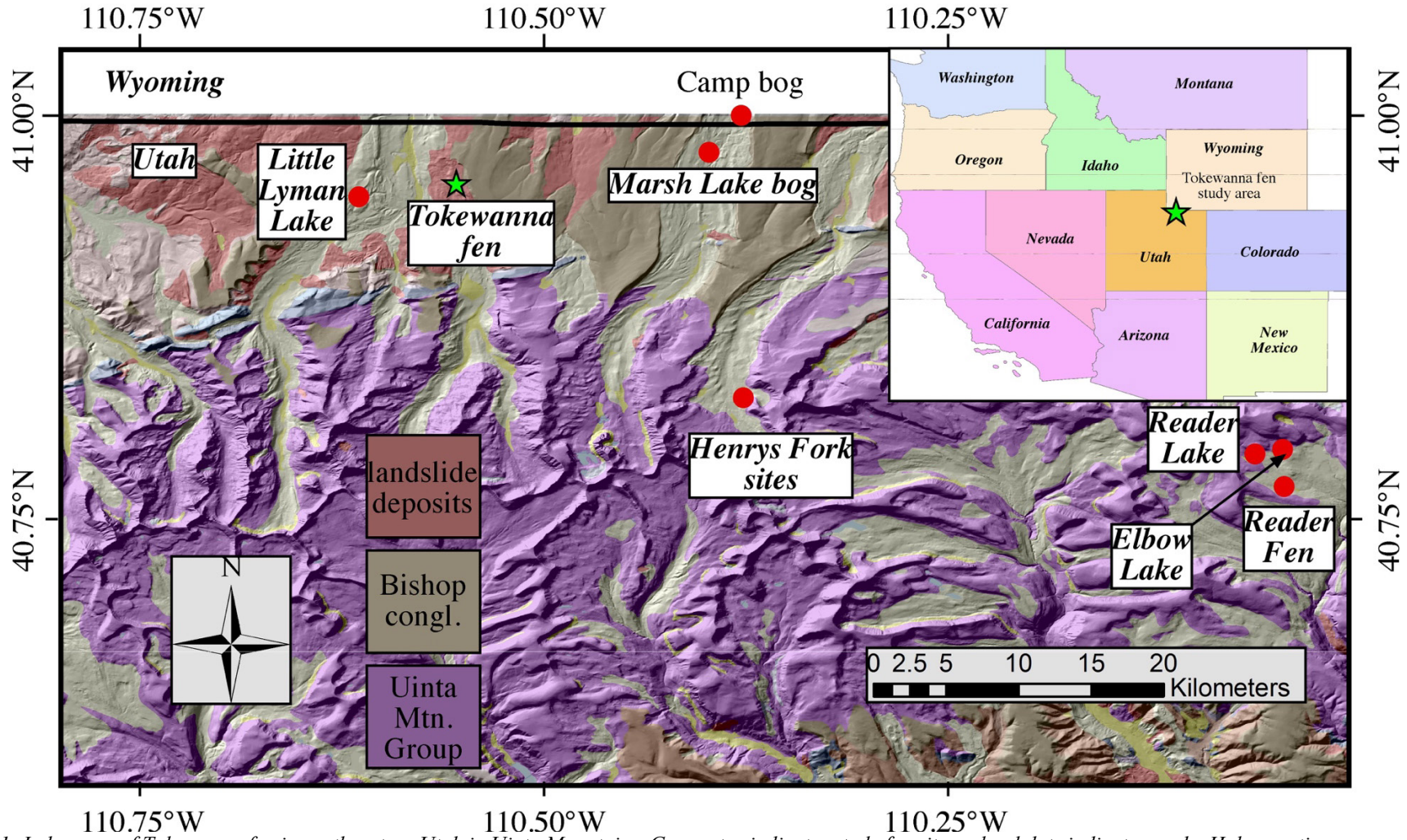

Figure 1: Index map of Tokewanna fen in northeastern Utah in Uinta Mountains. Green star indicates study fen site and red dots indicate nearby Holocene time climate study locations used for comparison. Lithologies are colored according to map legend. Latitude and longitude tick marks are indicated around the border and the map was generated in NAD 83.

Background

Site

The wetland is located between hummocks in a small basin (Fig. 2) that has presumably maintained its internal drainage since mass movement. Its mineral sediment source is primarily the surrounding hummocks and endogenous organic matter. A significant portion of its recharge is from groundwater and it is a peat-accumulating wetland, therefore it is considered a fen (Mitsch & Gosselink, 1993; Bedford and Godwin, 2003). The catchment created should have a mostly undisturbed depositional record that can be used for sampling and climate proxy analysis. Its elevation is 2,923 meters and the core location is: latitude 40.958592, longitude -110.554259 as identified in Figure 2.

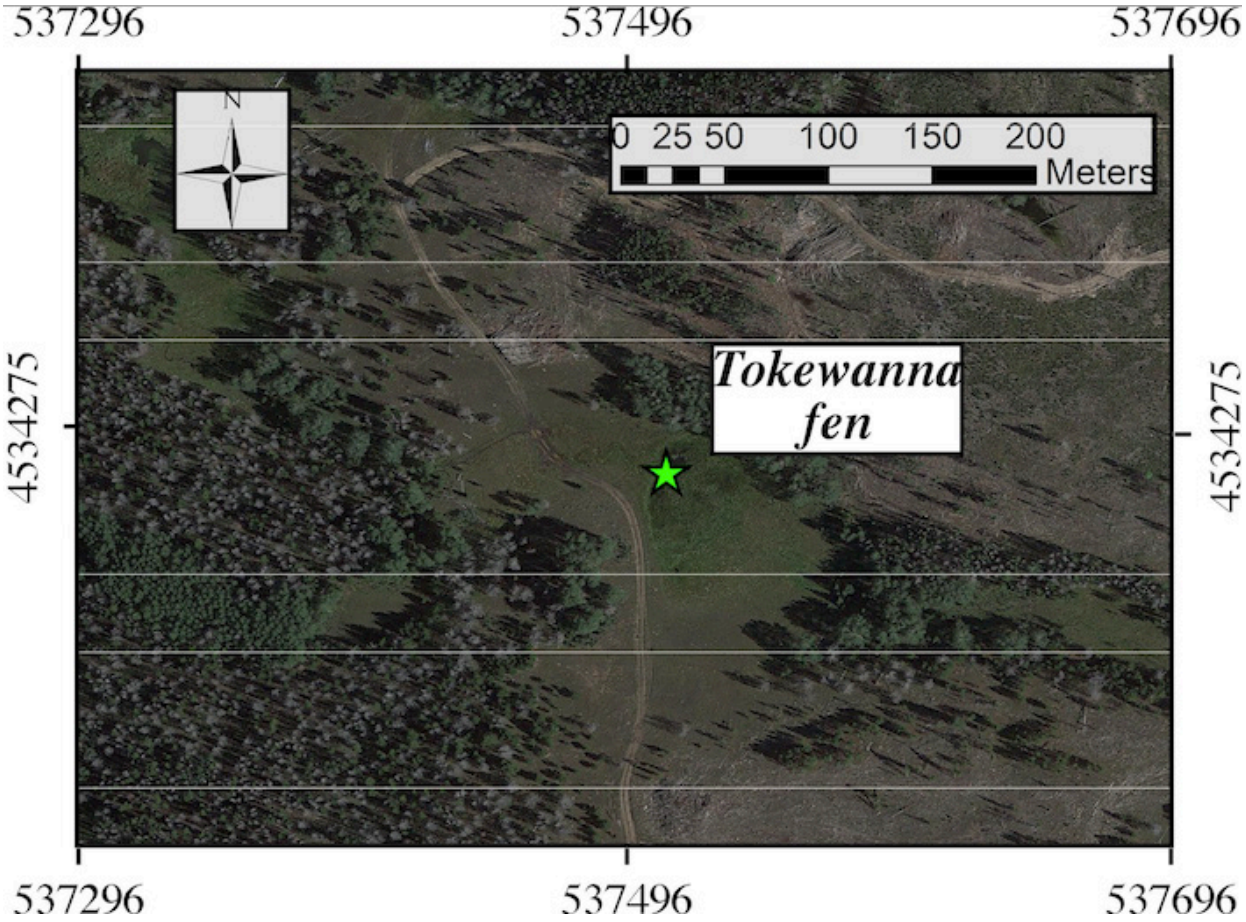

Figure 2: Image of study fen. Core location is 40.958592, -110.554259, identified by green star. The fen encompasses the area of light green vegetation surrounding the core location. The trees to the NE are upslope and on raised hummocks. Outlining tick marks are in UTM meters from NAD 83.

Magnetic Susceptibility as a Climate Indicator

Magnetic susceptibility measures the propensity of sediments to become magnetized (Thompson et al., 1975). Increased magnetic susceptibility readings in fen sediment would indicate higher clastic input, as endogenous organic matter has a very low magnetic susceptibility. When used in conjunction with other proxy data, magnetic susceptibility can provide strength and understanding to other proxy records. An increase in clastic input in conjunction with drier vegetation could indicate increased windblown dust, for example.

Pyrolysis as a Climate Indicator

A recent review article by Baudin et al. (2015) describes the burgeoning uses of RockEval, a pyrolysis technique (Espitalie, 1985) within the oil and gas industry as well as environmental applications. Rock pyrolysis was originally designed for the oil and gas industry as a quick and inexpensive way to measure source rock maturity and generative potential (Espitalié et al., 1977, 1985a,b, 1986; Peters, 1986; Lafargue et al., 1998; Behar et al., 2001). Over subsequent decades it has been applied to recent sediments as well. Di Giovanni et al. (2000); Disnar et al. (2003) Hetényi et al. (2005), Sebag et al. (2006), Graz et al. (2012), Saenger et al. (2013), Hétényi and Nyilas (2014) used it to understand the nature of organic matter in soils; Copard et al. (2006), Poot et al. (2009) used it for detecting black carbon. Campy et al. (1994), Di Giovanni et al. (1998), Meyers and Lallier-Vergès (1999), Ariztegui et al. (2001), Steinmann et al. (2003), Jacob et al. (2004), Sanei et al. (2005), Boussafir et al. (2012), Zocatelli et al. (2012), Lavrieux et al. (2013), Sebag et al. (2013) and others have employed it to study recent lacustrine sediments. Peters and Simoneit (1982), Hussain and Warren (1991), Calvert et al. (1992), Combourieu-Nebout et al. (1999), Ganeshram et al. (1999), Ozcelik and Altunsoy (2000), Holtvoeth et al. (2001, 2003, 2005), Tamburini et al. (2003), Baudin et al. (2007, 2010), Kim et al. (2007), Marchand et al. (2008), Tribovillard et al. (2008, 2009), Biscara et al. (2011), Riboulleau et al. (2011), Hare et al. (2014), Hatcher et al. (2014), and others have applied it to

recent marine sediments. Van der Putten et al. (2008) applied it in multiproxy paleoclimate studies.

For this study of Holocene sediments, pyrolysis is used to identify hydrogen, oxygen, and total organic carbon. When dividing hydrogen by carbon and oxygen by carbon, they return the Hydrogen Index (HI) and Oxygen Index (OI) respectively, which are roughly equivalent to the H/C atomic ratio (Dembicki, 2009; Espitalie et al., 1977a; Peters, 1986; Baskin, 1997). HI readings can be correlated to typical organic source matter (Dembicki, 2009) and is used here to infer environmental conditions.

Plotting the Hydrogen Index against the Oxygen Index on a modified Van Krevelen diagram (Fig. 3) has been a common way to categorize the types of kerogen present in source rocks (Dembicki, 2009; Tissot et al., 1974; Espitalie et al., 1985; Peters, 1986). High H/C atomic ratios and low O/C atomic ratios, represented by high HI and low OI figures, are labeled Type I kerogens and are associated with lacustrine algal material. Moderate H/C and O/C atomic ratios are derived from autochthonous organic matter deposited in marine environments under reducing conditions and are labeled Type II kerogens. Type III kerogens are derived from terrestrial plant matter and have high O/C atomic ratios and low H/C atomic ratios. Type IV is a product of severe alteration and/or *in situ* oxidation and is essentially inert (Tissot and Welte, 1984; Tissot et al., 1974; Dembicki, 2009). These kerogen types can be used to indicate wetter or drier source matter existed at the Tokewanna fen by identifying source matter as algal or vascular plants.

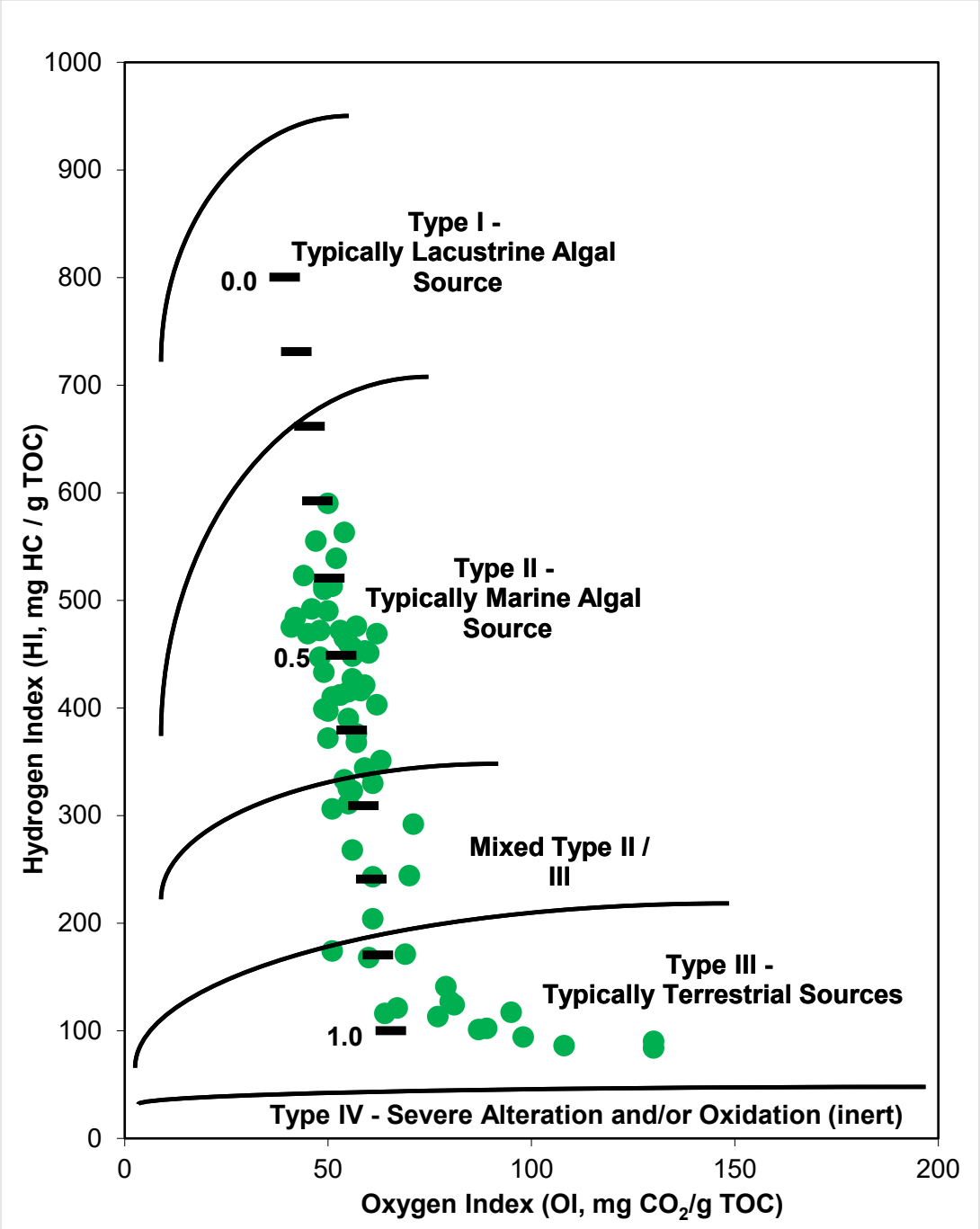

Figure 3: Pyrolysis results on a modified Van Krevelen diagram that delineates different kerogen types and is similar to the one initially proposed by Tissot et al. (1974). Samples are plotted in green and show a strong tendency towards the upper portion of the graph with higher HI values and lower OI values. The mineral matrix effect and mixing of organic material is likely lowering what would be higher HI values and is instead plotting samples in the marine algal source (Type II) area below the lacustrine algal (Type I) zone. Black bars indicate Type III kerogen mixing factors with 0.0 at 800 HI and 1.0 at 100 HI. Mixing model assumes no matrix effect and that all HI suppression is due to source matter mixing. Model suggests at least 30% Type III kerogen mixing in all samples, with many between 40% and 70%.

Biomass as Climate Indicator

The increase and decrease of biomass over time in response to changing climate can suggest increases and decreases in vegetation density. In this study, total organic content (TOC) as measured through pyrolysis is used as a measurement of biomass and an indication of changing conditions for vegetation. Higher percentages of TOC correlate to greater biomass abundance and more favorable growth conditions. When compared with magnetic susceptibility and pyrolysis, it can be used to further interpret environmental changes throughout the Holocene time at the Tokewanna fen.

Methods

Coring

A core was recovered near the fen margin (Appendix I). It was obtained in 8, 61 cm drives of a percussion corer until the device met refusal. Core sections were labeled drive 1, 2, etc.; sleeved in plastic; split 50/50; vacuum sealed; and refrigerated at 55 °F for storage. Five cm of sediment in the cutter head was not collected but is accounted for in the age/depth model.

Smear Slides

Smear slides were created following Myrbo (2013) at every visual lithologic change. Smear slides were then described following methods outlined by the National Lacustrine Core

Facility at the University of Minnesota (2011). Slides were used in conjunction with macroscopic descriptions to create a core log (Appendix I).

Lithology

The core lithology was grouped based on grain size and composition (Fig. 6). Mud/clay intervals were isolated, as were mud/clay with silt, and again isolated when containing sand. Peat intervals were then identified and divided based on clastic sediment grain size. These lithologic divisions were then given numeric values for statistical analysis. 1-3 are the intervals with only clastic sediments, and 4-7 are the intervals with peat.

^{14}C Ages

Sediment Samples

Eight organic-rich subsamples with roughly even spacing were chosen for ^{14}C ages. Organic richness was estimated by dark colored sediment and organic-rich material was selected for analysis. A 1 cm deep section of the sampling core half was collected with care to exclude sediment that was in contact with the core sleeve and potentially contaminated by smearing.

Care was taken to minimize the chance of sample contamination. New nitrile gloves were used between each sampling, the stainless-steel spatula was cleaned with deionized water and a Kimwipe between each use, and samples were carefully placed and capped in clean, 50 mL centrifuge tubes.

Samples were labeled by the drive number and core cradle reading at the uppermost sample contact. For example, label 3:32 indicates the sample is from drive 3 and the top of the sample is at 32 cm below the top of the sleeve. The samples analyzed were 1:27, 2:16, 3:32, 4:32, 5:41, 6:40, 7:42, 8:59.

CO2 Gas Preparation for Accelerator Mass Spectrometry and δ13CVPDB

Each sample was treated with an acid-base-acid wash of 10% HCl and 1.0M NaOH to remove potential carbonates and organic acids, similar to Brock et al. (2010). The samples were covered with HCl, and no effervescence was observed. Samples were then quickly rinsed with de-ionized water to stop reactions. The samples were then centrifuged at 2500 RPM for 2 minutes and the supernatant liquid decanted. Enough NaOH was then added to barely cover the sample and stirred with a glass stir rod, being left to react for less than a minute. The reaction was again stopped using deionized water and centrifuged at 2500 RPM. Again, the separated fluid was poured off. The final acid treatment and rinsing with deionized water followed the same procedure as before and samples then oven dried at 60 °C.

Approximately 1 g of dried sample was combusted to create CO_2 gas. Samples were placed in a quartz glass tube under vacuum to 600 °C. A low and constant oxygen flow volume was introduced in the vacuum line to support combustion. Two gas traps followed a dry ice-propanol slurry to collect water vapor, and liquid nitrogen for other gases including the CO_2 to be sampled. When the oven reached 600 °C, the sample was inspected for signs of complete

combustion – brick red and ashen coloring. If further combustion was needed, the sample was left under the oven. When combustion was complete, the gases frozen in the liquid nitrogen trap were isolated and cleaned using cryogenic methods. Between samples, the vacuum lines were evacuated, the quartz glass tube cleaned, and a new sample loaded.

Gases were further cleaned by passing over Cu and Ag metal heated to 600 °C. The copper was to strip NO_x from oxygen in the form of N_2. Silver reacts with sulfur to remove SO_2 gas. Again, gases were passed through a dry ice-propanol slurry water trap and condensed in a liquid nitrogen trap. Incondensible gases were pumped away. Finally, flame sealed CO_2 gas splits were labeled for accelerator mass spectrometry and $\delta^{13}C_{VPDB}$ analysis, sent, and analyzed at the Center for Applied Isotope Studies at the University of Georgia.

Ages in ^{14}C years were returned and converted to calibrated years before present (cal yr BP) using Calib 7.0 (Stuvier and Reimer, 2016), assuming the present as 1950 AD. Among calibrated results potential age ranges and 1 and 2 sigma (standard deviation) results were returned. Because of excursions in the calibration curve, more than one age range for a given sample is possible. Weighted averages were used with linear interpolation between them for calculating estimated ages (cal yr BP) of each pyrolysis sample. The high and low 2σ values were recorded each age range.

Magnetic Susceptibility

Before the core was analyzed for magnetic susceptibility, the drives were removed from 5 °C refrigeration and left for 24 hours to reach room temperature. Then, magnetic susceptibility was measured (Fig. 6) in 1 cm increments with a Bartington MS2C Core Logging Sensor at the Records of Environments and Disturbances lab at the University of Utah. Data collected are in relative SI units (Osleger et al., 2008).

Pyrolysis

Pyrolysis Operation

Pyrolysis was conducted at Brigham Young University (BYU) with a HAWK Workstation apparatus and, despite differences from the familiar Rock Eval apparatuses, operates similarly and produces comparable data. The HAWK Workstation and Rock Eval apparatus burns crushed samples in the absence of oxygen over a temperature ramp measuring hydrogen, oxygen, and carbon as they are evolved. It records the peak temperatures at which the maximum amount of hydrocarbons will be released from the rock or sediment. It also determines total organic carbon in the samples.

Like the Rock Eval 6, pyrolysis using the Hawk Workstation runs through two stages of combustion (Baudin et al., 2015). The first is a pyrolysis phase with a hydrogen carrier gas, and the second is an oxygenation phase with a helium carrier. A flame ionization detector is used during the pyrolysis phase to record peaks labeled S1 and S2. S1 indicates the amount of free hydrocarbon measured from volatilized hydrocarbon. Though these sediments are modern and

have not undergone thermal alteration or generated hydrocarbon, the results are used in TOC calculations. S2 indicates hydrocarbon generated from kerogen cracking during the temperature ramp. The S2 peak is used to determine a Hydrogen Index (HI), or the ratio of hydrogen to percent total organic carbon in the sample. In addition to the flame ionization detector is an infrared analyzer that is used to detect CO_2 and is recorded as an S3 peak (Espitalie et al., 1985; Peters, 1986).

Since rock pyrolysis was designed for source rock analysis in the petroleum industry, two significant changes for modern sediment analysis were needed (Baudin et al., 2015). It was necessary to start the temperature ramp at a lower temperature (180 °C instead of 300 °C) and to speed up the pyrolysis phase by 5 °C/min to 30 °C/min. The lower starting temperature was to evolve volatile organic matter that nature removes during source rock diagenesis, and the increased temperature ramp was to combine double S2 peak humps into one representing the aggregate organic matter. It is also worth noting the typical oxidation phase methods (Espitalie et al., 1985) were unchanged but run to 850 °C to calculate carbonate carbon, instead of 750 °C used by some instruments.

Sample Collection and Labeling

71 samples cut every 5 - 6 cm starting from core base were collected, including the 5 cm losses. Samples were taken from one core half while the other was archived. A potentially incomplete sample from the top of drive 4 was supplemented by an additional sample from the

bottom of drive 3.

Core halves were placed on a core cradle with a mounted meter stick for measurement. Samples were collected using a stainless-steel spatula. One end of the spatula was used to scrape the front surface of the core to ensure no contamination during core splitting would affect the sample. Afterwards, the other end of the spatula was used to collect a ~cubic centimeter of sediment. Samples were placed and kept in 3 dram vials with stopper tops to seal them. Between each sampling the spatula was cleaned as before.

Samples were labeled with the drive number and the measurement at the deepest sediment contact point. Sample 1:26 would be from drive 1 spanning the depth from 25 cm - 26 cm.

Dried Sample Homogenization

Following HAWK Workstation pyrolysis procedure, samples were freeze dried and crushed to pass through a 40 mesh (400 microns) nylon screen. The mesh screen was secured over a glass funnel and sediment transferred from an agate mortar through mesh and funnel into the sample's original vial. A stainless-steel spatula was used to scrape sediment from the mortar and through the mesh. Afterwards, mesh and funnel were cleaned with compressed air, bathed in 10% HCl for 10-20 minutes, rinsed with deionized water, and dried with compressed air. Mortar and pestle, and stainless steel spatula were rinsed and cleaned with deionized water, methanol, and Kimwipes.

Because modern rootlets penetrated the second and third samples from the surface (UMC-1 1:14, and UMC-1 1:20), these rootlets could skew the data. To remove modern rootlets, dried samples were lightly disaggregated and visible rootlets removed. This seemed to work well for the third sample down (UMC-1 1:20), but complete removal of rootlets for the second one down (UMC-1 1:14) is uncertain.

Approximately 20 mg of each sample was used for pyrolysis analysis following the methods of Baudin et al. (2015). Double humped S2 peaks were determined following the methods of Baudin et al. (washing with deionized water) to ensure they were not caused by salts.

Statistical Comparisons

Statistical analysis was used to compare measured data from the sampling locations to help identify relationships and strengthen interpretations. Any correlation coefficient >0.235 is marked "significant" based on the t-distribution (<0.05), and any correlation >0.305 is termed "very significant" based on the t-distribution (<0.01). The correlation table of the data used for Figure 6 is provided in Appendix III.

Results

Core Log

The core contains 3 main lithologies. Peat, varying combinations of silt and mud/clay, and combinations of peat and the silty mud/clay. The mud is primarly feldspathic with ~25% clays, which are dominated by smectite group minerals as revealed by two reconnaissance. Sand

also appears in two horizons. Terms to describe the composition proportions analyzed microscopically using smear slides are: dominant (>50%), abundant, (25-50%), common (5-25%), rare (1-5%), and trace (<1%). The upper 137 cm (composite depth) are mainly silt with minor peat. The remainder of the core is dominated by peat with varying silt and mud/clay mixed. Minor intervals lacking peat are present, including the bottom of the core. Results are illustrated in Appendix I. The lithologic changes also have very significant correlations to magnetic susceptibility, biomass balance, and HI values.

^{14}C Ages

Age/cumulative depth relations are illustrated in Figure 4 with the surface used for age 0. The base of the core at a calculated depth of 455 cm returned the oldest calibrated age of ~11,027 cal yr BP – the present being 1950. All samples are in stratigraphic order, except for one that was omitted from the model. The sample labeled 1:27 at a calculated depth of 20 cm depth returned a modern age. This is likely from homogenization of sediment from grazing, the effects of which can be observed on the modern fen surface.

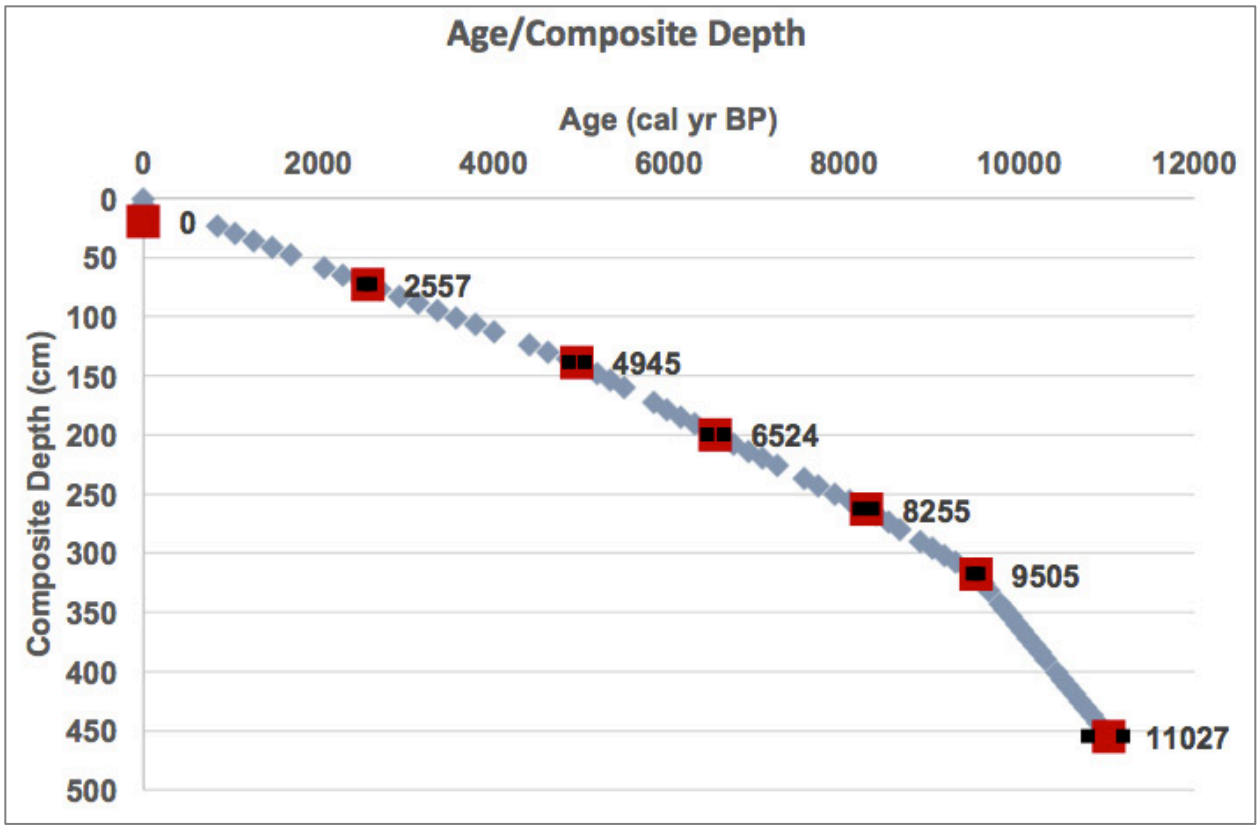

Figure 4: Age/composite depth curve with orange squares indicating measured ^{14}C ages, and blue diamonds indicating calculated sample ages from linear interpolation. Two black squares at each measured site indicate the 2σ high and low cal yr BP calculation. Initial rates of deposition were higher until ~9505 cal yr BP, with a final rate decrease ~4945 cal yr BP.

Magnetic Susceptibility

Magnetic susceptibility is illustrated in Figure 6. The values range from -2 to 15 SI units with most higher values in the upper 73 cm (composite depth), ~2557 cal yr BP. One large excursion exists between 370 cm and 376 cm (composite depth), ~1082-10150 cal yr BP. The data are very significant when correlated to pyrolysis, TOC, and lithology.

Pyrolysis

Oscillations from lower to higher HI values are indicated throughout the Tokewanna fen's depositional history (Fig. 5). These variations in HI values signify changes from Type III kerogens of primarily terrestrially sourced organic matter, to Type II kerogens of apparent marine algal origins. HI values range from a low of 84 mg HC/TOC to a high of 590 mg HC/TOC. When plotted on a modified Van Krevelen diagram (Fig. 3) (similar to Tissot et al., 1974) with kerogen origin cutoffs in place, the data plot in a reciprocal function arc from Type II through Type III. There clearly is no significant source of marine algal organic matter in this fen. The origin of Type II organic matter will be discussed below.

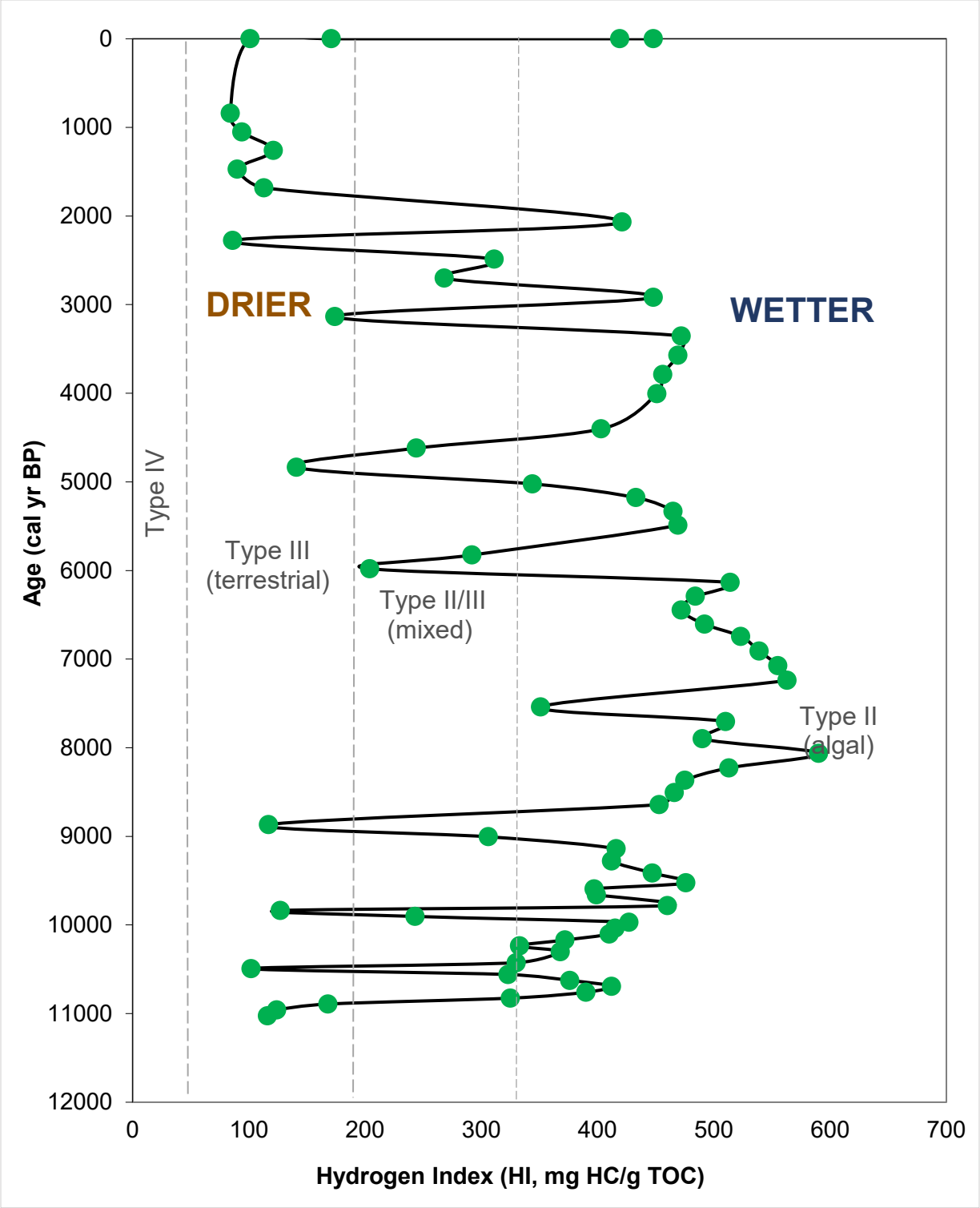

Figure 5: Plot of the Hydrogen Index (HI) from pyrolysis of each sample to age cal yr BP. Samples with lower HI values are from a drier environment dominated by terrestrial plant matter. Samples with higher HI values are from a wetter environment. HI readings are influenced by mixing and the mineral matrix effect (see text) that suppress higher HI values. Trends, however, are real and therefore instructive. Wetter conditions prevailed through much of the Holocene time, punctuated by brief drier periods. Dry spikes mimic magnetic susceptibility spikes, confirming increased clastic input. Drier conditions have prevailed from ~1350 cal yr BP – modern, with two uppermost samples recording current wetter conditions.

Biomass Balance

The TOC measurements fluctuate throughout the Holocene Epoch (Fig. 6) between a high of 35.8% and a low 1.4%. The low is reached at the base of the core ~11,027 cal yr BP, and the high ~8,369 cal yr BP. From ~3,359 cal yr BP to present the highest TOC percentage recorded is 12.5%, with 9 of the 16 points under 4%. These TOC highs and lows act as proxy for biomass abundance.

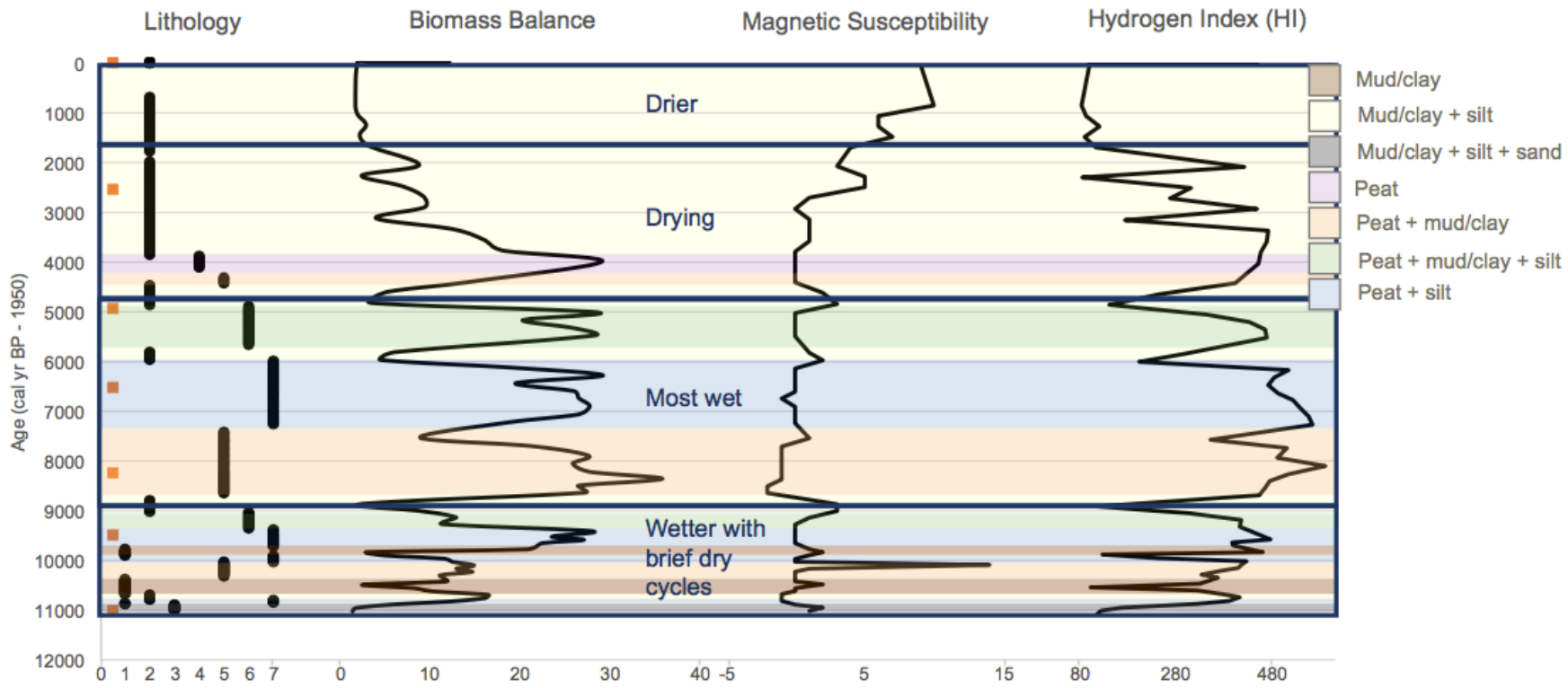

Figure 6: Four isolated time intervals outlined in blue with climate interpretations in blue text. Curves described from left to right. Age of horizon – orange squares indicate measured ^{14}C locations. Lithologic differences numbered with values 1-3 not containing peat, and 4-7 containing peat; numbered lithologies are also colored as indicated. Biomass balance as measured by percent TOC with higher values correlating to greater organic matter density. Magnetic susceptibility measured in relative units (SI) indicating increased in clastic sediment input with higher values. Hydrogen index curve measured in mg HC/g TOC, with higher values correlating to wetter conditions and lower values correlating to drier conditions.

Discussion

Quaternary Climate Records

The north slope of the Uinta Mountains is replete with evidence of Pleistocene glaciation. Cirques, U-shaped valleys, moraines, and glacial lakes and ponds make up much of the landscape. Though heavily glaciated during the Pleistocene Epoch, no glaciers are present today. Late-Pleistocene deglaciation started by 16 ka cal yr BP and was completed by 14-15 ka cal yr BP (Munroe et al., 2006; Munroe, 2002; Laabs et al., 2009). This deglaciation coincides with the falling Bonneville shoreline to the west (Benson et al., 2011).

Multiple Quaternary pollen records have been studied in the Uinta Mountains and the adjacent Rocky Mountain region (Briles et al., 2012; Fall et al., 1995; Feiler et al., 1997; Jiménez-Moreno and Anderson, 2012; Krause and Whitlock, 2013; Koll, 2012; Lynch, 1998; Mensing et al., 2012; Minckley et al., 2012; Munroe, 2003; Vierling, 1998). Most recently, Louderback et al. (2015) studied pollen records from cores of bogs on the north side of the Uinta range along the Utah-Wyoming border; the Camp Bog and the Marsh Lake Bog near the Tokewanna fen study site (Fig. 1). The bogs record major vegetation shifts at the end of the last glaciation ~11,700-11,200 cal yr BP, also at ~8200 cal yr BP. These shifts match larger regional variations recorded in the Rocky Mountains (Louderback et al., 2015). The first is associated with post-Younger Dryas event warming and/or greater effective moisture. The second vegetation shift was attributed by Louderback et al. (2015) to be climatically driven with slightly

warmer temperatures or slightly less annual precipitation. Generally, greater extremes in winter/summer temperatures existed during the early Holocene Epoch relative to today (Shurtliff et al., 2016) with warming and/or greater effective moisture peaking around the middle Holocene time with temperatures ~1 °C warmer than modern (Louderback, 2015; Munroe, 2003), followed by cooling (Munroe, 2003).

Regionally, the Uinta Mountains are affected by two major climate regimes. There is a summer-dry/winter-wet regime affecting the northwestern USA, including Washington, Oregon, Idaho, and Montana. It is caused by a summer buildup of a high-pressure system in the eastern Pacific Ocean creating an anticyclone that suppresses precipitation (Munroe, 2003). The second major regional climate regime is a summer-wet/winter-dry regime of the southwestern USA. Upwind mountain ranges and high plains limit winter precipitation, while monsoonal events bring in moisture from the Gulf of Mexico during the summer (Munroe, 2003). The Uinta Mountains lie at a boundary for these conditions and may display even precipitation through summer and winter (Munroe, 2003).

Locally, precipitation is driven primarily by topography (Munroe, 2002). During the winter months as the high-pressure system of the eastern Pacific Ocean subsides, precipitation is carried inland and deposited on the windward side of mountains. Eastward trending storms likely deliver greater precipitation on west facing slopes like the Tokewanna Landslide, though a site-specific study has not verified this. An additional weather phenomenon directly related to

topography and common in this intermountain west area are winter inversions (Wolyn and McKee, 1989; Whiteman, 2000) that potentially affect local moisture and vegetation patterns (Patten, 1963). Louderback et al. (2015) noted them as cause for potential climatic patchiness in the Uinta Mountains.

Core Log

The coring location was nearer the margin of the fen than in the depocenter. This allowed for greater sensitivity to variations in wetter and drier conditions. During wetter times the pond would be larger with increases in algal matter. During drier conditions, the pond would contract and support increased terrestrial plant matter near the margins where the core was taken. Were the core to be in the depocenter expanding and contracting signals of the pond margins might be lost or suppressed.

A hand-augured, ~14.2 m deep well was later installed nearer the depocenter. Roughly, the top 0.6 m appeared to be clay, the middle ~3.5 m peat, and the final 0.1 m clay. The study core displayed more lithologic variation (Appendix I) because it was near the fen margin capturing expanding and contracting pond conditions. The very significant correlations between lithologies, HI values, and biomass balance confirm the importance of the core location to detect changes in wetter and drier conditions.

These very significant correlations, as well as the very significant correlation to magnetic susceptibility, help interpret the environment and main clastic depositional sources. Peat layers

are associated with wetter conditions, and clastic sedimentation spikes generally mark drier conditions. Increases in clastic sedimentation during drier times also suggests most non-organic sedimentation was from windblown systems. Increasing magnetic susceptibility during wetter periods would suggest pluvial activity the dominant clastic sedimentation factor, and increased detrital grain sizes would be expected.

^{14}C

Three general rates of deposition are observed from the onset of sedimentation that suggest slowing deposition rates. Initial rates of sedimentation from ~11,000 - 9,945 cal yr BP are the greatest at ~0.900 mm/yr; then from ~9,505 - 4,945 cal yr BP rates decrease to ~0.393 mm/yr; and decrease again from ~4,945 cal yr BP until today to ~0.281 mm/yr. The slowing from ~4,945 cal yr BP coincides with drying conditions. Perhaps sediment shedding into the basin was a greater factor at the fen's inception, but as the basin filled, less and less sediment was captured by the basin from overland flow and windblown dust became the dominant deposition mechanism.

Pyrolysis

Potential for Error

The HI/OI plots are useful for kerogen typing but are not without potential error. Espitalie et al. (1980), Katz (1983), Espitalie et al. (1984), Dembicki (1992, 2009), and Calvert (2004) illustrated a mineral matrix effect where a cracked pyrolysate forming carbonized residue

(coke) that is retained by the sample and does not contribute to the S2 peak. This effect is most common in a clay matrix, like many of the samples in this study. Langford and Blanc-Valleron (1990) showed how plotting S2 vs. TOC and performing a linear regression can help identify if this is the case for a given set of samples. The method requires a high degree of confidence (high R^2) and affirms that a positive x-intercept indicates kerogen adsorbed onto mineral grains (Langford and Blanc-Valleron, 1990).

While such a plot for this study does cross the x-axis at 2.4% TOC (Fig. 7), these samples do not adhere to a critical assumption. Langford and Blanc-Valleron (1990) require of only a single source of organic matter input. Instead, this study assumes two main sources of organic input; one from terrestrial plant matter, and the other from lacustrine algal material. Calvert (2004) adds mixing of organic matter with one hydrogen poor source as another reason for the S2/TOC regression x-intercept. It is likely that this fen location has had a near continual mix of organic input. It is shallow enough and small enough transiently that hydrogen poor, terrestrial plant matter (Type III) could have always had a presence, while the amount of aquatic algal (Type I) would vary. This mixing matches Calvert's (2004) additional reason for the x-intercept.

Evidence for mixing would be expected in pyrolysis results as outlined by Dembicki (2009). He illustrated how mixing of Type I organic matter with Type III would dilute the hydrogen signal and, depending on the percentage of each input, may plot as Type II. This is probably the case in this study because there are no samples plotting in the Type I region where

lacustrine algal material would be. Instead, many are plotting in the Type II region that is associated with marine organic material. Marine organic matter obviously does not fit the depositional setting. Instead, a mixture of Type III and Type I organic matter may result in many samples plotting in the Type II field.

The data suggest the positive x-intercept of the S2/TOC linear regression is both from organic matter mixing and from the mineral matrix effect. Because many of the samples contain clay, adsorption of kerogen would occur and the mixture of aquatic algal material and terrestrial plant matter would be important. What is uncertain is the degree to which each is affecting the HI/OI ratios and their respective plots on the modified Van Krevelen diagram (Fig. 3). Proposed in Figure 3 is a Type III kerogen mixing model. The model assumes no matrix effect and suggests general percentages of Type III kerogen sources affecting Type I sources. All samples indicate at least 30% Type III kerogen (terrestrial) sources with many plotting between 40% and 70%. Mixing percentages are exaggerated because of the mineral matrix effect affecting the sample.

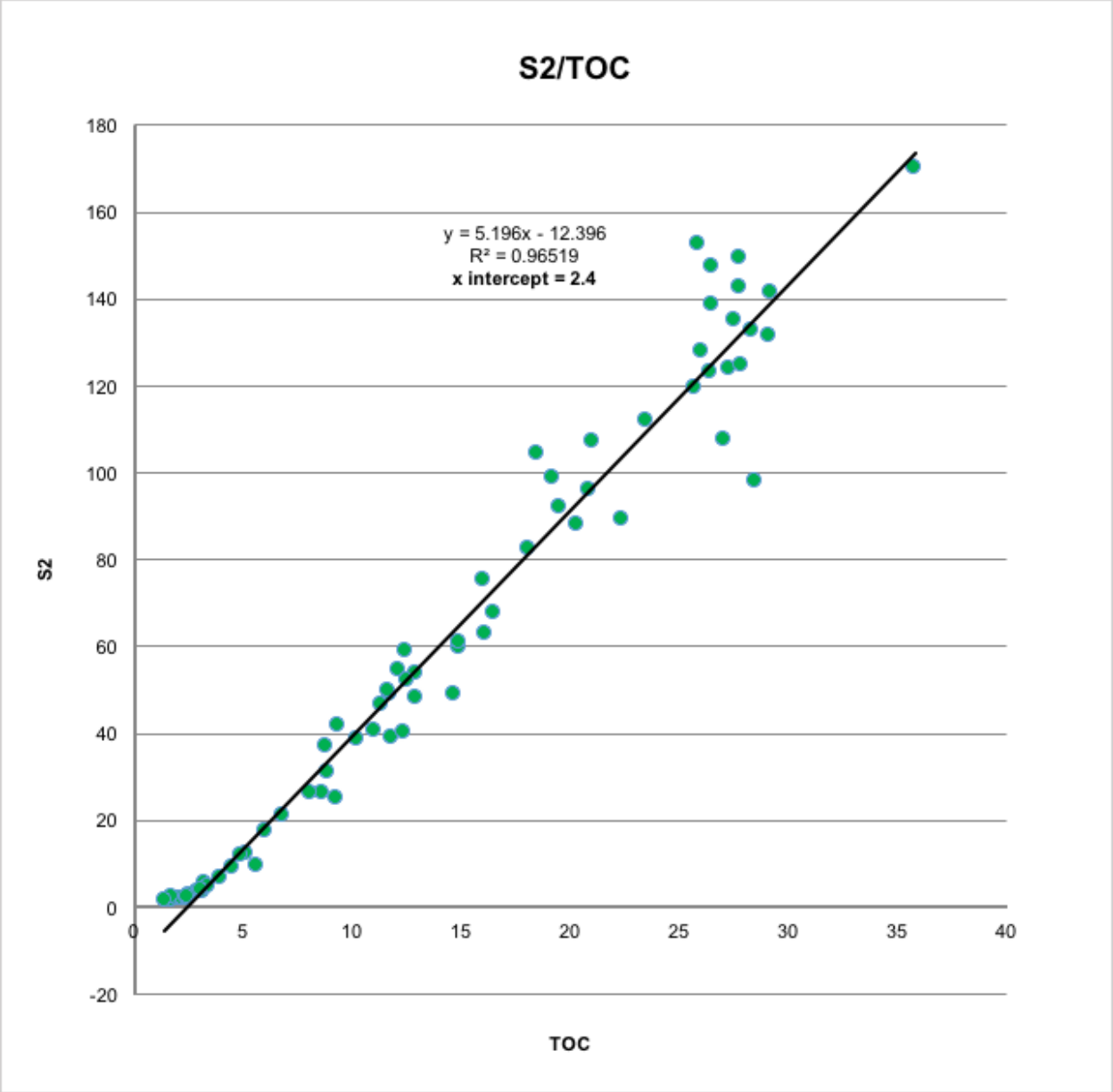

Figure 7: A linear regression of pyrolysis data with a strong correlation plotting all samples with S2 to TOC (total organic content). The x axis is crossed at 2.4 instead of the origin. This indicates the matrix effect is present in the samples that artificially lowers the Hydrogen Index (HI) readings (Langford and Blanc-Valleron, 1990). Kerogen source type mixing also can lower the HI values (Calvert, 2004). The mixing at the Tokewanna Fen is likely suppressing upper HI values significantly.

In addition to mixing, an effort to isolate and identify the mineral matrix effect of the Type III samples is presented. It can be assumed the samples plotted as Type III kerogens are not

affected significantly by mixing with Type I kerogens as the mixing model suggests 90-100% Type III sources. Figure 8 shows the S2/TOC regression for the Type III kerogen samples, isolated as those with HI <200. Because organic matter mixing is less apparent in these samples, the x-intercept can be more strongly correlated to kerogen adsorption. The S2/TOC x-intercept lies at a positive 1.0% TOC, implying a mineral matrix effect. Langford and Blanc-Valleron (1990) recommend removing organic matter and measuring elemental hydrogen and carbon mathematically to eliminate the mineral matrix effect. Following their methods (Langford and Blanc-Valleron,1990) the x intercept was removed and new HI values calculated (S2 / (TOC - x_intercept) * 100). This increases HI values such that shift most points plot in the mixed kerogen zone (Fig. 9). Samples greater than 200 HI and excluded from this correction are presumably from sources mixed to the point that isolating and correcting for the matrix effect with this method is unreliable. For this reason, another method for identifying the mineral matrix effect and correcting for it should be used for samples with HI values greater than 200.

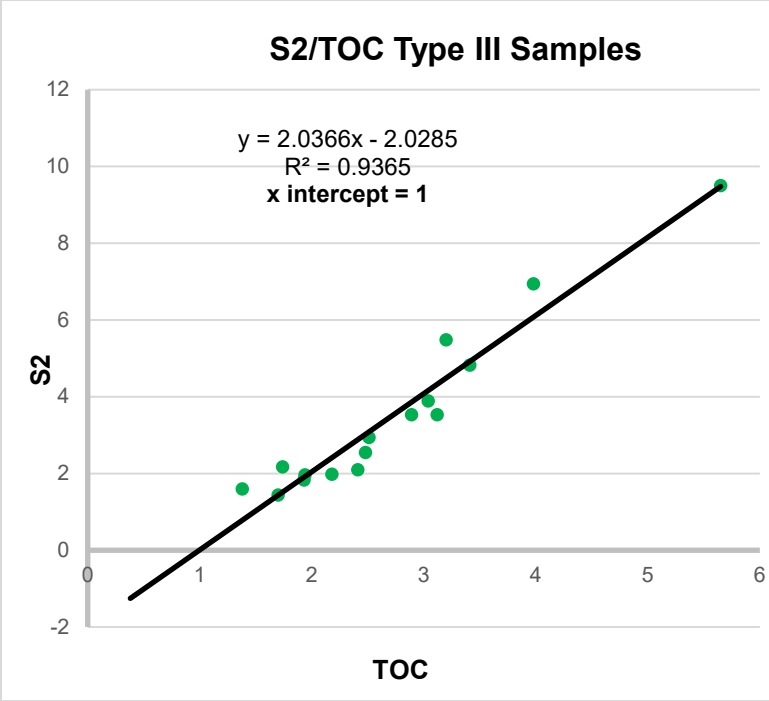

Figure 8: Lower pyrolysis HI values, Type III kerogen, samples are considered less affected by kerogen source type mixing. The samples plotted are those from the Type III zone of Figure 3 and are plotted with S2 against TOC (total organic content). The positive x intercept of the linear regression indicates a matrix effect (Langford and Blanc-Valleron, 1990).

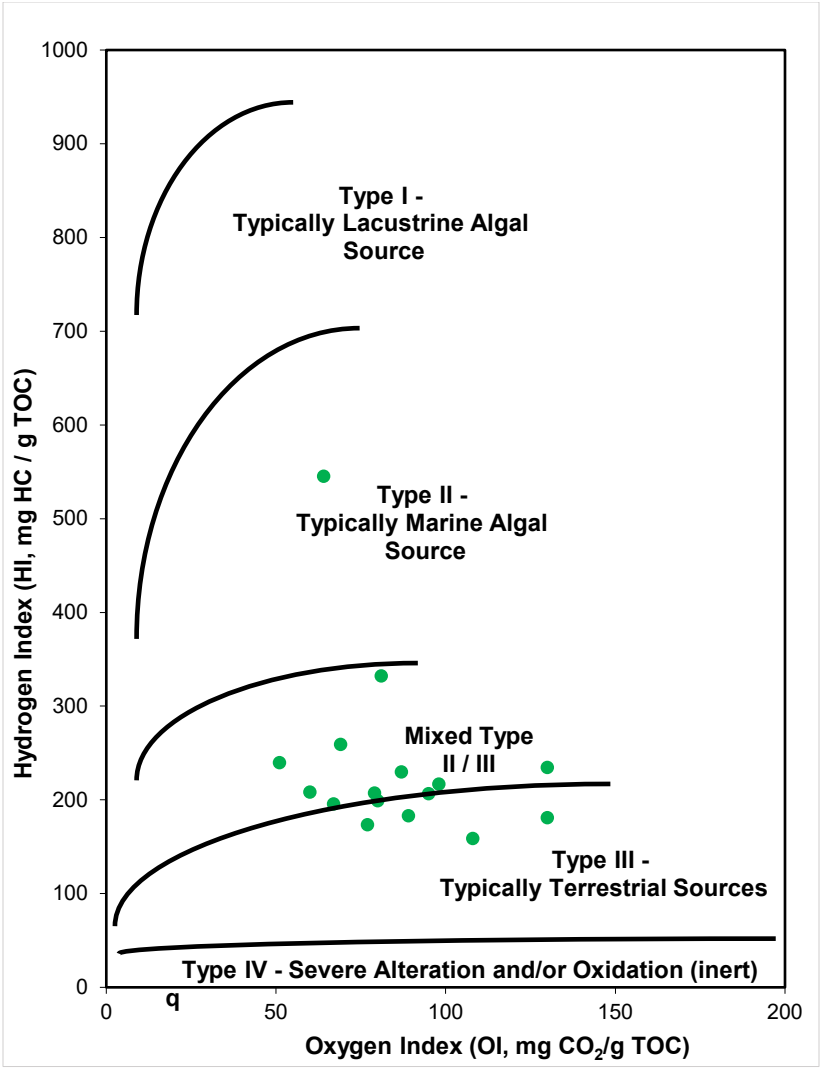

Figure 9: Type III pyrolysis samples (identified with HI <200) plotted on the modified Van Krevelen (similar to Tissot et al. 1974) diagram after applying the matrix correction suggested by Langford and Blanc-Valleron (1990). The data plot with higher HI values, counteracting the adsorption of kerogen to mineral grains in the matrix effect.

Significance of Pyrolysis Results

Despite the mineral matrix effect and the effects of organic matter mixing in the samples, the variations are significant. Samples from the coring location that plot on the HI/OI modified Van Krevelen diagram (Fig. 3) with higher HI values experienced wetter conditions than those plotting with lower HI values because higher HI values indicate greater algal input. Consistent variation in samples shows changes in the combination of lacustrine algal material and terrestrial plant matter. Drier conditions are marked with terrestrial dominant kerogens (Type III) and are less frequent than times dominated by wetter conditions indicated as Type II kerogens. Increased controls on the level of mixing and the matrix effect would be instructive, yet the values as plotted already indicate shifts in environmental conditions that may be used for comparison to other proxy data from the core, and previous regional studies.

When the Hydrogen Index is plotted against age with kerogen type delineated (Fig. 5), 48 of the data points plot in the wetter Type II area, 10 plot in the transition Type II/III area, and 16 plot in the drier Type III area. When a curve is fit to the data points, samples oscillate with depth between Type II and Type III kerogens with occasional transition points in the Type II/III area. From first sedimentation, most the samples represent a wetter environment, punctuated by brief drier spells. Conditions seem to have been even wetter from ~8,800 - 4,800 cal yr BP where no sample crosses into the drier Type III zone and samples plot further into the wetter Type II zone. From ~4,800 - 1350 cal yr BP conditions trend toward drier overall conditions while maintaining

wetter oscillations. ~1350 cal yr BP marks a significant drier trend that persists until the present. The two uppermost samples are also of modern age but suggest return to a wetter environment, similar to that observed between ~8,800 cal yr BP and ~4,800 cal yr BP.

The wetter and drier conditions suggested by lower and higher Hydrogen Index values are supported by other data. Magnetic susceptibility increases correlate with drier conditions, as do decreases in the biomass balance. Drier conditions would increase mineral dust input, detected by magnetic susceptibility, and create less favorable growing conditions, which might increase mineral sediment input during overland flow. Another check on wet versus dry climate conditions was made. Samples of high and low HI index were cleaned and examined. The low HI index sample was devoid of siliceous algal microfossils, whereas the high HI index sample contained abundant chrysophyte cysts, indicative of wet conditions.

Comparison Sites

The Tokewanna fen pyrolysis data, though oscillatory indicates wet and dry trends through Holocene time. Using the Hydrogen Index/Age graph (Fig. 5) as a guide, the trends are separated into four climate zones and compared to other nearby study locations. The first zone is from ~11,000 - 8,800 cal yr BP, the second is from ~8,800 - 4,800 cal yr BP, the third is from ~4,800 - 1,700, and the fourth is from ~1,700 - present. The climate records compared by nearest proximity are: from Little Lyman Lake by Tingstad et al. (2011); Marsh Lake Bog and Camp

Bog by Louderback et al. (2015); upper Henry's Fork basin by Munroe (2003); Reader and Elbow lakes by Corbett and Munroe (2010); and Reader Fen by Koll (2012) (Fig. 1).

Little Lyman Lake is on the opposing side of the glacial valley of Blacks Fork from the Tokewanna fen. It is 5.2 km westward and lies at nearly the same elevation. Tingstad et al. (2011) reconstructed a 13,000-year history there using diatom analysis. This is the only study site that is west of the Tokewanna fen, and likely the best analog for what is observed in the Tokewanna fen core.

Marsh Lake Bog and Camp Bog lie eastward 13 km and northward 2, and 5 km of the Tokewanna fen. Here, Louderback et al. (2015) analyzed charcoal records and accumulated a pollen record from a core at each bog to infer vegetation shifts. These study sites are in the East Fork of Smiths Fork, a major stream drainage.

Upper Henry's Fork basin studied by Munroe (2003) is roughly 14 km east and 15 km south of the Tokewanna fen. Here, he collected clastic and organic sediments from two cutbanks in streams above modern timberline. Pollen records and ^{14}C ages were then used to understand the Holocene timberline history.

Reader and Elbow Lakes are about 43 km east and 17 km south of Tokewanna fen where Corbett and Munroe (2010) compared these two nearby lakes of nearly identical conditions and elevations. They are in the headwaters of the Whiterocks River, and unlike the previously described locations, they are along the southern slopes of the Uinta Mountains. Cores were taken

from each lake and loss-on-ignition, carbon to nitrogen ratios, biogenic silica content, and sediment grain size were used to understand reactions to climate change.

Reader Fen, studied by Koll (2012), is also on the southern side of the Uinta Mountains about 2.5 km south of Reader and Elbow Lakes. The Reader Basin watershed is composed of upper, middle, and lower fen accumulating meadows retained by glacial till downslope (Koll, 2012). From a core taken here, she used magnetic susceptibility, charcoal, and pollen analysis to reconstruct a Holocene time fire, vegetation, and climate history.

~11,000 - 8,800 cal yr BP

From 11,000 - 8,800 cal yr BP, Tokewanna fen pyrolysis records cycle from low Hydrogen Index (HI) values to high, with HI values increasing each cycle. Low valued HI cycles were brief and quickly switch back to higher. These data suggest this period was initially drier and became increasingly wetter.

Little Lyman Lake records indicate this as a warming period (Tingstad et al., 2011). Louderback et al. (2015) identified a shift from alpine Artemesia-birch steppe to open spruce park-land at the Marsh Lake and Camp bogs during this time, which indicates increases in temperature and/or decreases in effective moisture. The upper Henry's Fork basin vegetation development indicate mean July temperatures were ~1 °C greater than modern by 9,500 cal yr BP (Munroe, 2003). Starting from ~10,000 to ~ 6,000 cal yr BP Reader and Elbow lakes experienced a dramatic increase in precipitation (Corbett and Munroe, 2010). Corbett and

Munroe (2010) think this may be driven by an insolation maximum that increased monsoonal circulation. Koll's study at Reader Fen also suggests this as a wet period, except with cooler temperatures. She concludes this from the *Picea- Artemisia* steppe vegetation that developed just after deglaciation (Koll, 2012).

~8,800 - 4,800 cal yr BP

Between 8,800 - 4,800 cal yr BP pyrolysis HI values continue to cycle, with higher HI values each cycle until ~8,060 cal yr BP. Local maximum HI values then steadily decline with each cycle. Despite the decline in wetter period HI values after ~8,060 cal yr BP, the drier periods are not as dry as others; no data plot in the Type III kerogen (driest) zone, as in previous and subsequent cycles. Increased wetness throughout each cycle is inferred from these data.

Across the valley, the Little Lyman Lake record does not change throughout this period but continues to indicate warming throughout the middle Holocene Epoch (Tingstad et al., 2011). Tingstad et al. (2011) identify shifts in diatoms at 8,200 - 6,500 cal yr BP and 5,000 - 3,500 cal yr BP that could be attributed to an increase in precipitation. At 8,400 cal yr BP the Marsh Lake and Camp bogs began to shift from spruce-Artemisia parkland to lodgepole pine forest (Louderback at al., 2015). Louderback et al. (2015) believe these shifts to be caused by an increase of winter temperatures by 1-2 °C, slightly less annual precipitation, or a combination of the two. At Henry's Fork basin, continued warming was observed through the middle Holocene time. This was signified by a shift from *Pinus* to *Picea* parkland, with a maximum warmth

reached shortly after ~5,500 cal yr BP and back near modern temperatures ~1,000 years later (Munroe, 2003). Precipitation at Reader and Elbow lakes decreased from ~6,000 - 4,000 cal yr BP (Corbett and Munroe, 2010). The Reader Fen record suggests enhanced monsoons from ~8,500 - 3,200 cal yr BP with increased warming becoming influential by ~7,500 cal yr BP, as marked by a vegetation shift (Koll, 2012).

Carson et al. (2007) documented bankfull flood records on the north flank of the Uinta Mountains that show a 10-15% increase in larger floods from ~8,500 - 5,000 cal yr BP. They attribute the increase to higher temperatures and increased seasonality of solar radiation that favored accumulation and rapid melting of deep snowpack. Tingstad et al. (2011) attribute possible precipitation increases at Little Lyman Lake to increased snowpack and winter runoff, or greater rainfall in the summer.

Each of these local records suggests a warming and/or increased precipitation throughout the middle Holocene time. Though warming and cooling trends cannot be inferred directly from pyrolysis data, increased effective moisture can and is indicated at the Tokewanna fen by increases in HI values. The higher HI values agree with the wetter trends during the middle Holocene Epoch, and data from these other studies suggest it to be warmer during this period as well.

~4,800 - 1,700 cal yr BP

This period is marked in the Tokewanna fen as trending towards a drier environment with some HI values again plotting in the Type III (driest) region. Climate swings are still apparent with the wetter periods dominating the time interval. HI values become progressively lower in the wet zone however, indicating the drying trend.

The interval from ~ 4,800 - 1,700 cal yr BP, inferred by pyrolysis, overlaps a warm to cool boundary from Little Lyman Lake. It occurs at ~3,500 cal yr BP and is demonstrated by a diatom shift associated with cooler temperatures (Tingstad et al., 2011). By this time both Marsh Lake Bog and Camp Bog had completely switched to lodgepole pine forests that continue until today (Louderback et al., 2015). That shift, as mentioned above, would have required warmer winter temperatures, or slightly less annual precipitation (Louderback et al., 2015). The record from Henry's Fork basin suggests temperatures over this period stabilized to near modern conditions (Munroe, 2003). The records however do not extend beyond ~3,800 cal yr BP. The decreased precipitation regime of Reader and Elbow lakes turned to a severe drought from ~4,000 - 2,700 cal yr BP (Corbett and Munroe, 2010). After ~2,700 cal yr BP precipitation resumed with the possibility of a shift in the seasonality of precipitation (Corbett and Munroe, 2010). The Reader Fen record marks this time interval as still affected by the increased monsoon season with evidence for greater temperatures and precipitation (Koll, 2012).

~1,700 - modern cal yr BP

~1,700 cal yr BP marks the beginning of a sustained drier trend not seen elsewhere in the Tokewanna fen core. HI values are low and prolong until modern times. The uppermost 4 sample locations are calculated to be modern, but the top 2 samples indicate wetter conditions again with higher HI values.

It may be possible that the wetter conditions indicated are only facilitated by organic matter growing in a hoof print, but these higher HI data indicating a return to middle Holocene Epoch conditions are seen elsewhere. Tingstad et al. noted that the uppermost data point of Little Lyman Lake indicates a recent return of diatom species assemblages towards something more like those of the mid-Holocene time (2011). This is particularly significant in validating the two uppermost Tokewanna fen samples because of the proximity of Little Lyman Lake.

The remaining interval from ~1,700 cal yr BP to modern, at Little Lyman Lake the taxa indicate a cooler environment, attributed to lower temperatures (Tingstad et al., 2011). Marsh Lake Bog and Camp Bog continued to sustain lodgepole pine (Louderback et al., 2015), meaning conditions must have remained somewhat stable. The same can be said of upper Henrys Fork basin (Munroe, 2003). Reader and Elbow lakes continued their post-drought shift back to wetter conditions (Corbett and Munroe, 2010). That record is unclear as to the amount or pattern of precipitation, but Koll's record (2012) from Reader Fen is more precise. At Reader Fen, the warming trend switched to a cooling and drying trend ~900 cal yr BP and remained until present.

She notes the cooling and drying trend is relative to the mid-Holocene Epoch and still represents temperatures and precipitation greater than today.

Regional Comparisons Summary

Little Lyman Lake; upper Henrys Fork basin; Reader Lake, Elbow Lake; and Reader Fen all show a warming during the middle Holocene time; with one possibility for the shift to lodgepole pine at Marsh Lake Bog and Camp Bog being mid-Holocene Epoch warming. The most commonly cited reason for the warming is from increased insolation (Corbett and Munroe, 2010; Koll, 2012; Munroe, 2003). Although not always the case in the Uinta Mountains (Munroe, 2003; Louderback et al., 2015), most of the Holocene time increases in temperature are associated with at least periods of added moisture (Corbett and Munroe, 2010; Koll, 2012; Tingstad et al., 2011). Munroe notes that regional insolation changes can drive local changes in the seasonal precipitation distribution (2003). This understanding helps to reconcile some of the nearby records with periods of increased warming not reflecting increased precipitation. The rain shadow tempering northern slope precipitation from Gulf monsoons may also contribute to these variations.

As it stands, the Tokewanna fen record does not directly indicate warming or cooling. However, because nearby records indicate warming and increased precipitation (Koll, 2012; Corbett and Munroe, 2010; Tingstad et al., 2011), the mid-Holocene Epoch increase in

precipitation likely relate to an increase in temperature. If this true, wetness record reflects similar warming and cooling trends of nearby studies.

Correlation attempts between the Tokewanna HI values and Koll's fire record at Reader Fen (Koll, 2012), and with various curves from the Little Lyman Lake study (Tingstad et al., 2011) were made. No comparison offered a significant R, however visual similarities exist between the Little Lyman Lake percent plankton record and the Hydrogen Index record of the Tokewanna fen (Fig. 10). Two general trends of increased percent plankton at Little Lyman Lake can be seen from ~8,800 cal yr BP to ~6,000 cal yr BP, and from ~5,300 cal yr BP to ~2,900 cal yr BP. These excursions roughly match increases in Hydrogen Index values at the Tokewanna fen, adding validity to the interpretation of increased wetness indicated by increased HI readings.

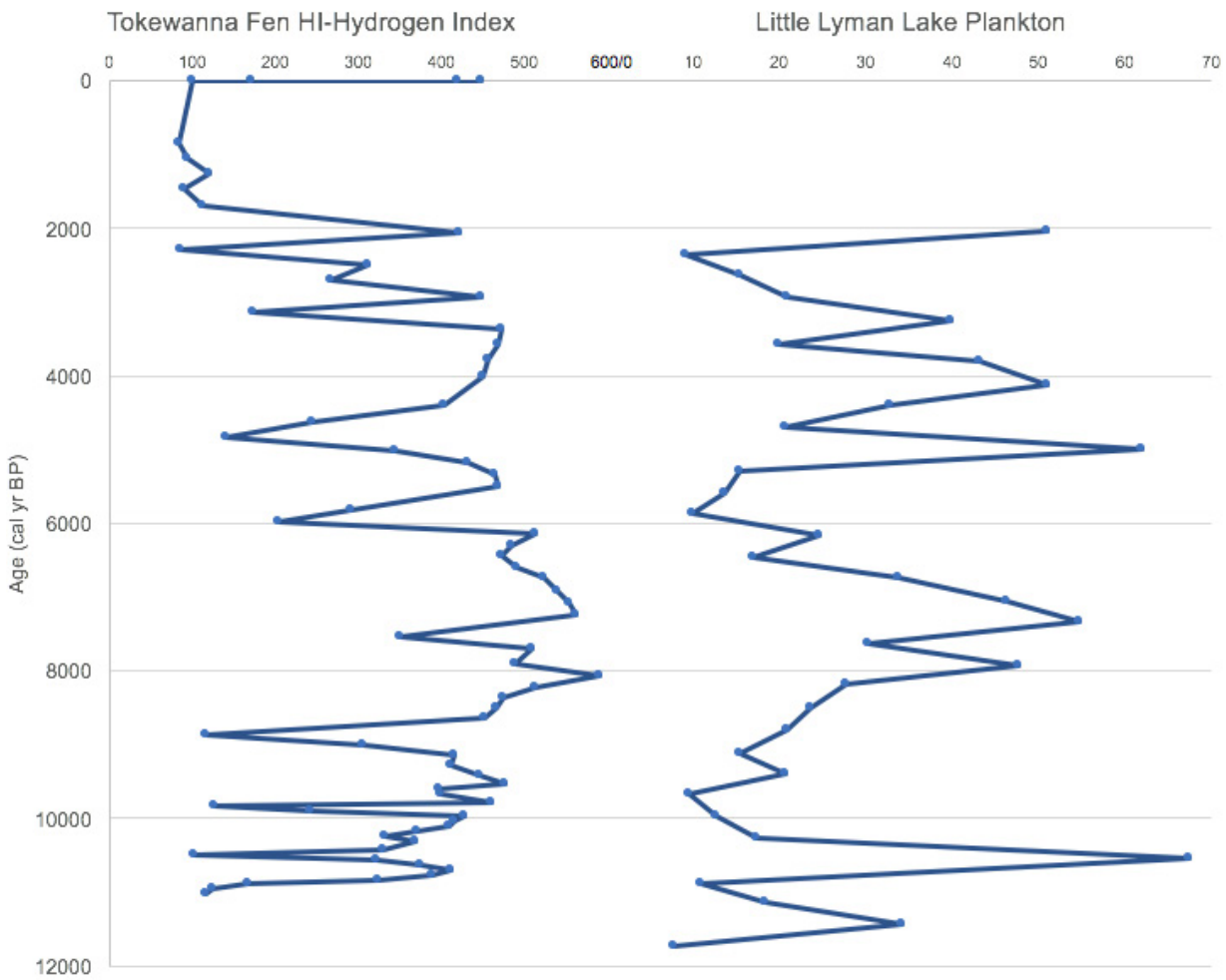

Figure 10: A side-by-side view of the Tokewanna HI/age record and the Little Lyman Lake plankton/age record (Tingstad et al., 2011). HI values are in HC/g TOC and plankton values are in percent. Two general excursion between ~8,800 - 6,000 cal yr BP, and ~5,300 – 2,900 cal yr BP in percent plankton roughly match HI increase excursions. The plankton record adds confidence to the HI record of wetter conditions during times of increased HI readings at the Tokewanna fen.

Important factors that may contribute to the differences in the Tokewanna fen record and comparison studies are the climate proxy methods used, local topography, and sample density. Because the vegetation detected by pyrolysis is that of seasonal wetland vegetation, it is more sensitive to climate change than the tree pollen records used in most of the comparison studies. The diatom record of Little Lyman Lake is the only record more sensitive to climate changes

than the pyrolysis record. Topographic variation between compared studies can drive precipitation variance, as with rain shadows. Also, the frequent sample interval of the Tokewanna fen core captures more climate variation than some of the other studies. Ideally, all comparisons would be from records with the same amount of data points, from samples at the same time intervals

Because of the size of the Tokewanna slide and its distance from Quaternary faults, increased precipitation appears to have been the reason for slope failure and that a wetness record during initial sedimentation at the Tokewanna fen would reflect that. What the record indicates instead is an initially drier environment that became increasing wet through the middle Holocene time with a maximum wetness reached at ~8,060 cal yr BP. Conditions then became progressively drier.

The most likely explanation for this is that the core represents an incomplete history for this fen. The Little Lyman Lake record shows an initial organic layer that looks like peat ~12,800 cal yr BP (Tingstad et al., 2011). Because that lake is across the glacial valley and even closer to the glacial head, post-glacial conditions, including sedimentation, should have occurred very near ~12,800 cal yr BP at Tokewanna fen. Also, the observed lithology when a piezometer was augured in the depocenter varied much less. Because the core was taken near the edge of the fen where it would be more sensitive to changing conditions, it likely provides an incomplete sedimentation history and therefore an incomplete climate record.

Conclusion

The Uinta Mountains, Utah are an east - west trending range of Laramide age with a neo-Proterozoic-age core. It has been highly glaciated on the north and south slopes and displays numerous landslides across the range. One such slide is the Quaternary Tokewanna Landslide on the northern slopes. This landslide is of significant size and is presumably too far from a Quaternary fault to have been triggered by an earthquake. Understanding the climate history since the slide moved may point to increased moisture as the cause for the slope failure.

Between its hummocks is small basin supporting a fen system (Tokewanna fen). To understand the climate history since the slide movement, a core was taken from the Tokewanna fen for proxy analysis. The proxy methods to be used were sediment pyrolysis, biomass variation via TOC records, and magnetic susceptibility. 7 ^{14}C ages were obtained to create and time/depth curve. The pyrolysis, biomass, and magnetic susceptibility results have complementing records that indicate wetter and drier conditions through the Holocene aged core.

Climate conditions from the Tokewanna fen were divided into 4 intervals and compared to nearby studies in the Uinta Mountains. At the Tokewanna fen:

~11,000 - 8,800 cal yr BP - Starts drier and quickly oscillates between wet and dry, with significantly shorter drier periods than wetter. Moisture oscillations trend wetter during this time.

~8,800 - 4,800 cal yr BP – The wetter trend continues with suppressed drier cycles. Maximum wetness is marked at ~8,060 cal yr BP and is followed by a decrease in wetter cycle magnitude.

~4,800 - 1,700 cal yr BP - A drying trend continues. Climate oscillations continue to have longer wetter cycles.

~1,700 cal yr BP - modern - A strong and sustained drier signal occurs until the core top that return to wetter conditions.

Comparison of Uinta Mountains climate studies suggest a warming trend during the mid-Holocene time with some of them associating increased moisture. It is assumed the increase in the Tokewanna fen moisture during the Holocene Epoch is related to these regional increases in temperature. The wetter and drier cycles of the Tokewanna fen do not indicate an initial wet period that was hypothesized to be the trigger for the Tokewanna Landslide. However, it is likely the coring location did not capture the first sedimentation in the catchment because it was taken near the fen margin, and a more complete record may yet indicate wetter conditions during the early Holocene time when the slope likely failed.

References

Ariztegui, D., Chondrogianni, C., Lami, A., Guilizzoni, P., and Lafargue, E., 2001, Lacustrine organic matter and the Holocene paleoenvironmental record of Lake Albano (central Italy): Journal of Paleolimnology, v. 26, p. 283-292.

Baudin, F., Combourieu-Nebout, N., and Zahn, R., 2007, Organic signatures of rapid climaticchanges in Western Mediterranean during North Atlantic cold events of the Last Glacial: Bulletin Société Géologique De France, v. 178, p. 3-13.

Baudin, F., Disnar, J., Aboussou, A., and Savignac, F., 2015, Guidelines for Rock–Eval analysis of recent marine sediments: Organic Geochemistry, v. 86, p. 71-80.

Baudin, F., Disnar, J., Martinez, P., and Dennielou, B., 2010, Distribution of the organic matter in the channel-levees systems of the Congo mud-rich deep-sea fan (West Africa). Implication for deep offshore petroleum source rocks and global carbon cycle: Marine and Petroleum Geology, v. 27, p. 995-1010.

Bedford, B.L., and Godwin, K.S., 2003, Fens of the United States: distribution, characteristics, and scientific connection versus legal isolation: Wetlands, v. 23, p. 608-629.

Behar, F., Beaumont, V., and Penteado, H.D.B., 2001, Rock-Eval 6 technology: performances and developments: Oil & Gas Science and Technology, v. 56, p. 111-134.

Benson, L., Lund, S., Smoot, J., Rhode, D., Spencer, R., Verosub, K., Louderback, L., Johnson, C., Rye, R., and Negrini, R., 2011, The rise and fall of Lake Bonneville between 45 and 10.5 ka: Quaternary International, v. 235, p. 57-69.

Biscara, L., Mulder, T., Martinez, P., Baudin, F., Etcheber, H., Jouanneau, J., and Garlan, T., 2011, Transport of terrestrial organic matter in the Ogooué deep sea turbidite system (Gabon): Marine and Petroleum Geology, v. 28, p. 1061-1072.

Boussafir, M., Sifeddine, A., Jacob, J., Foudi, M., Cordeiro, R.C., Albuquerque, A.L.S., Abrao, J., and Turcq, B., 2012, Petrographical and geochemical study of modern lacustrine sedimentary organic matter (Lagoa do Caço, Maranao, Brazil): Relationship between early diagenesis, organic sedimentation and lacustrine filling: Organic Geochemistry, v. 47, p. 88-98.

Bradfield, T.D., 2007, Pre-Historic Landslides on the Southeast Flank of the Uinta Mountains, Utah: Character and Causes of Slope Failure: .

Briles, C.E., Whitlock, C., and Meltzer, D.J., 2012, Last glacial–interglacial environments in the southern Rocky Mountains, USA and implications for Younger Dryas-age human occupation: Quaternary Research, v. 77, p. 96-103.

Calvert, S., Bustin, R., and Pedersen, T., 1992, Lack of evidence for enhanced preservation of sedimentary organic matter in the oxygen minimum of the Gulf of California: Geology, v. 20, p. 757-760.

Campy, M., Bichet, V., DIGIOVANNI, C., Richard, H., Richard, J., and Olive, P., 1994, Evolution of the matter fluxes since 12,000 years in the high Doubs valley (France): Bulletin De La Société Géologique De France, v. 165, p. 381-400.

Combourieu Nebout, N., Londeix, L., Baudin, F., Turon, J., Von Grafenstein, R., and Zahn, R., Quaternary marine and continental paleoenvironments in the western Mediterranean (Site 976, Alboran Sea): palynological evidence, *in* Proceedings of the Ocean Drilling Program. Scientific Results, , Ocean Drilling Program, p. 457-468.

Copard, Y., Di-Giovanni, C., Martaud, T., Albéric, P., and Olivier, J., 2006, Using Rock-Eval 6 pyrolysis for tracking fossil organic carbon in modern environments: implications for the roles of erosion and weathering: Earth Surface Processes and Landforms, v. 31, p. 135-153.

Corbett, L.B., and Munroe, J.S., 2010, Investigating the influence of hydrogeomorphic setting on the response of lake sedimentation to climatic changes in the Uinta Mountains, Utah, USA: Journal of Paleolimnology, v. 44, p. 311-325.

Dembicki Jr, H., 2009, Three common source rock evaluation errors made by geologists during prospect or play appraisals: AAPG Bulletin, v. 93, p. 341-356.

Di-Giovanni, C., Disnar, J., Bakyono, J., Kéravis, D., Millet, F., and Olivier, J., 2000, Determination of eroded geological formations using organic matter characterization

(Moulin basin, Alpes-de-Haute-Provence, France). Comptes Rendus De l'Academie Des Sciences Series IIA Earth and Planetary Science, v. 331, p. 7-14.

di-Giovanni, C., Disnar, J.R., Bichet, V., Campy, M., and Guillet, B., 1998, Geochemical characterization of soil organic matter and variability of a Postglacial detrital organic supply (Chaillexon Lake, France): Earth Surface Processes and Landforms, v. 23, p. 1057-1069.

Disnar, J., Guillet, B., Keravis, D., Di-Giovanni, C., and Sebag, D., 2003, Soil organic matter (SOM) characterization by Rock-Eval pyrolysis: scope and limitations: Organic Geochemistry, v. 34, p. 327-343.

Espitalié, J., Deroo, G., and Marquis, F., 1985, La pyrolyse Rock-Eval et ses applications. Deuxième partie. Revue De l'Institut Français Du Pétrole, v. 40, p. 755-784.

Espitalié, J., Laporte, J.L., Madec, M., Marquis, F., Leplat, P., Paulet, J., and Boutefeu, A., 1977, Méthode rapide de caractérisation des roches mètres, de leur potentiel pétrolier et de leur degré d'évolution: Revue De l'Institut Français Du Pétrole, v. 32, p. 23-42.

Espitalie, J., Deroo, G., and Marquis, F., 1986, La pyrolyse Rock-Eval et ses applications. Troisième partie. Revue De l'Institut Français Du Pétrole, v. 41, p. 73-89.

Fall, P.L., Davis, P.T., and Zielinski, G.A., 1995, Late quaternary vegetation and climate of the Wind River Range, Wyoming: Quaternary Research, v. 43, p. 393-404.

Feiler, E.J., Anderson, R.S., and Koehler, P.A., 1997, Late Quaternary paleoenvironments of the White River Plateau, Colorado, USA: Arctic and Alpine Research, p. 53-62.

Ganeshram, R.S., Calvert, S.E., Pedersen, T.F., and Cowie, G.L., 1999, Factors controlling the burial of organic carbon in laminated and bioturbated sediments off NW Mexico: Implications for hydrocarbon preservation: Geochimica Et Cosmochimica Acta, v. 63, p. 1723-1734.

Graz, Y., Di-Giovanni, C., Copard, Y., Mathys, N., Cras, A., and Marc, V., 2012, Annual fossil organic carbon delivery due to mechanical and chemical weathering of marly badlands areas: Earth Surface Processes and Landforms, v. 37, p. 1263-1271.

Hansen, W.R., 2005, The Geologic Story of the Uinta Mountains: Globe Pequot, .

Hare, A.A., Kuzyk, Z.Z.A., Macdonald, R.W., Sanei, H., Barber, D., Stern, G.A., and Wang, F., 2014, Characterization of sedimentary organic matter in recent marine sediments from Hudson Bay, Canada, by Rock-Eval pyrolysis: Organic Geochemistry, v. 68, p. 52-60.

Hatcher, P.G., Ravin, A., Behar, F., and Baudin, F., 2014, Diagenesis of organic matter in a 400 m organic rich sediment core from offshore Namibia using solid state 13 C NMR and FTIR: Organic Geochemistry, v. 75, p. 8-23.

Hetényi, M., and Nyilas, T., 2014, Soil organic matter characterization using S3 and S4 signals from Rock-Eval pyrolysis: Pedosphere, v. 24, p. 563-574.

Hetényi, M., Nyilas, T., and Toth, T., 2005, Stepwise Rock-Eval pyrolysis as a tool for typing heterogeneous organic matter in soils: Journal of Analytical and Applied Pyrolysis, v. 74, p. 45-54.

Holtvoeth, J., Wagner, T., Horsfield, B., Schubert, C., and Wand, U., 2001, Late-Quaternary supply of terrigenous organic matter to the Congo deep-sea fan (ODP site 1075): implications for equatorial African paleoclimate: Geo-Marine Letters, v. 21, p. 23-33.

Holtvoeth, J., Kolonic, S., and Wagner, T., 2005, Soil organic matter as an important contributor to late Quaternary sediments of the tropical West African continental margin: Geochimica Et Cosmochimica Acta, v. 69, p. 2031-2041.

Holtvoeth, J., Wagner, T., and Schubert, C.J., 2003, Organic matter in river-influenced continental margin sediments: The land-ocean and climate linkage at the Late Quaternary Congo fan (ODP Site 1075): Geochemistry, Geophysics, Geosystems, v. 4, .

Hussain, M., and Warren, J.K., 1991, Source rock potential of shallow-water evaporites: An investigation in holocenepleistocene Salt Flat sabkah (playa), west Texas-New Mexico: Carbonates and Evaporites, v. 6, p. 217-224.

Ingamells, C., 1970, Lithium metaborate flux in silicate analysis: Analytica Chimica Acta, v. 52, p. 323-334.

Jacob, J., Disnar, J., Boussafir, M., Sifeddine, A., Turcq, B., and Albuquerque, A.L.S., 2004, Major environmental changes recorded by lacustrine sedimentary organic matter since

the last glacial maximum near the equator (Lagoa do Caçó, NE Brazil): Palaeogeography, Palaeoclimatology, Palaeoecology, v. 205, p. 183-197.

Jiménez-Moreno, G., and Anderson, R.S., 2012, Pollen and macrofossil evidence of Late Pleistocene and Holocene treeline fluctuations from an alpine lake in Colorado, USA: The Holocene, p. 0959683612450199.

Kim, J., Park, M., Tsunogai, U., Cheong, T., Ryu, B., Lee, Y., Han, H., Oh, J., and Chang, H., 2007, Geochemical characterization of the organic matter, pore water constituents and shallow methane gas in the eastern part of the Ulleung Basin, East Sea (Japan Sea): Island Arc, v. 16, p. 93-104.

Koll, R.A., 2012, Long-Term Vegetation, Climate, and Fire History in the Eastern Uinta Mountains, Utah, USA [M.S. thesis]: Salt Lake City, University of Utah .

Krause, T.R., and Whitlock, C., 2013, Climate and vegetation change during the late-glacial/early-Holocene transition inferred from multiple proxy records from Blacktail Pond, Yellowstone National Park, USA: Quaternary Research, v. 79, p. 391-402.

Laabs, B.J., Refsnider, K.A., Munroe, J.S., Mickelson, D.M., Applegate, P.J., Singer, B.S., and Caffee, M.W., 2009, Latest Pleistocene glacial chronology of the Uinta Mountains: support for moisture-driven asynchrony of the last deglaciation: Quaternary Science Reviews, v. 28, p. 1171-1187.

Lafargue, E., Marquis, F., and Pillot, D., 1998, Rock-Eval 6 applications in hydrocarbon exploration, production, and soil contamination studies: Revue De l'Institut Français Du Pétrole, v. 53, p. 421-437.

Lambert, F., Delmonte, B., Petit, J., Bigler, M., Kaufmann, P.R., Hutterli, M.A., Stocker, T.F., Ruth, U., Steffensen, J.P., and Maggi, V., 2008, Dust-climate couplings over the past 800,000 years from the EPICA Dome C ice core: Nature, v. 452, p. 616-619.

Lavrieux, M., Disnar, J., Chapron, E., Bréheret, J., Jacob, J., Miras, Y., Reyss, J., Andrieu-Ponel, V., and Arnaud, F., 2013, 6700 yr sedimentary record of climatic and anthropogenic signals in Lake Aydat (French Massif Central): The Holocene, p. 0959683613484616.

Louderback, L.A., Rhode, D., Madsen, D.B., and Metcalf, M., 2015, Rapid vegetation shifts in the Uinta Mountains (Utah and Wyoming, USA) during the Late Pleistocene and Holocene: Palaeogeography, Palaeoclimatology, Palaeoecology, v. 438, p. 327-343.

Lowe, J.J., and Walker, M.J., 2014, Reconstructing quaternary environments: Routledge, .

Lynch, E.A., 1998, Origin of a park–forest vegetation mosaic in the Wind River Range, Wyoming: Ecology, v. 79, p. 1320-1338.

MacDonald, G.M., and Tingstad, A.H., 2007, Recent and multicentennial precipitation variability and drought occurrence in the Uinta Mountains region, Utah: Arctic, Antarctic, and Alpine Research, v. 39, p. 549-555.

Mahowald, N., Kohfeld, K., Hansson, M., Balkanski, Y., Harrison, S.P., Prentice, I.C., Schulz, M., and Rodhe, H., 1999, Dust sources and deposition during the last glacial maximum and current climate: A comparison of model results with paleodata from ice cores and marine sediments: Journal of Geophysical Research: Atmospheres, v. 104, p. 15895-15916.

Marchand, C., Lallier-Verges, E., Disnar, J., and Kéravis, D., 2008, Organic carbon sources and transformations in mangrove sediments: a Rock-Eval pyrolysis approach: Organic Geochemistry, v. 39, p. 408-421.

Mensing, S., Korfmacher, J., Minckley, T., and Musselman, R., 2011, A 15,000 year record of vegetation and climate change from a treeline lake in the Rocky Mountains, Wyoming, USA: The Holocene, p. 0959683611430339.

Meyers, P.A., and Lallier-Vergès, E., 1999, Lacustrine sedimentary organic matter records of Late Quaternary paleoclimates: Journal of Paleolimnology, v. 21, p. 345-372.

Minckley, T.A., Shriver, R.K., and Shuman, B., 2012, Resilience and regime change in a southern Rocky Mountain ecosystem during the past 17 000 years: Ecological Monographs, v. 82, p. 49-68.

Mitsch, W., and Gosselink, J., 1993, Wetlands Van Nostrand Reinhold: New York, v. 722, .

Munroe, J.S., 2005, Glacial geology of the northern Uinta Mountains: .

Munroe, J.S., 2003, Holocene timberline and palaeoclimate of the northern Uinta Mountains, northeastern Utah, USA: The Holocene, v. 13, p. 175-185.

Munroe, J.S., 2003, Estimates of Little Ice Age climate inferred through historical rephotography, northern Uinta Mountains, USA: Arctic, Antarctic, and Alpine Research, v. 35, p. 489-498.

Munroe, J.S., Laabs, B.J., Shakun, J.D., Singer, B.S., Mickelson, D.M., Refsnider, K.A., and Caffee, M.W., 2006, Latest Pleistocene advance of alpine glaciers in the southwestern Uinta Mountains, Utah, USA: evidence for the influence of local moisture sources: Geology, v. 34, p. 841-844.

Munroe, J.S., and Mickelson, D.M., 2002, Last glacial maximum equilibrium-line altitudes and paleoclimate, northern Uinta Mountains, Utah, USA: Journal of Glaciology, v. 48, p. 257-266.

Murray, R., Miller, D.J., and Kryc, K., 2000, Analysis of major and trace elements in rocks, sediments, and interstitial waters by inductively coupled plasma–atomic emission spectrometry (ICP-AES): .

Myrbo, A., 2013, Making smear slides: (https://tmi.laccore.umn.edu/module/blogpost?postURL=https%3A%2F%2Fwww.googleapis.com%2Fblogger%2Fv2%2Fblogs%2F8153395487262690384%2Fposts%2F77004203033260329101/5 2015).

National Lacustrine Core Facility, 2011, Tool for microscopic identification: (https://tmi.laccore.umn.edu/1/5 2014).

Osleger, D.A., Zierenberg, R.A., Suchanek, T.H., Stoner, J.S., Morgan, S., and Adam, D.P., 2008, Clear Lake sediments: anthropogenic changes in physical sedimentology and magnetic response: Ecological Applications, v. 18, .

Ozcelik, O., and Altunsoy, M., 2000, Organic Facies Characteristics of Quaternary Sediments, Gulf of Izmit, Marmara Sea, Turkey: International Geology Review, v. 42, p. 1017-1029.

Patten, D.T., 1963, Vegetational pattern in relation to environments in the Madison Range, Montana: Ecological Monographs, v. 33, p. 375-406.

Peters, K., 1986, Guidelines for evaluating petroleum source rock using programmed pyrolysis: AAPG Bulletin, v. 70, p. 318-329.

Peters, K., and Simoneit, B., 1982, ROCK-EVAL PYROLYSIS OF QUATERNARY SEDIMENTS FROM LEG-64, SIT-479 AND SITE-480, GULF OF CALIFORNIA: Initial Reports of the Deep Sea Drilling Project, v. 64, p. 925-931.

Poot, A., Quik, J.T., Veld, H., and Koelmans, A.A., 2009, Quantification methods of Black Carbon: Comparison of Rock-Eval analysis with traditional methods: Journal of Chromatography A, v. 1216, p. 613-622.

Riboulleau, A., Tribovillard, N., Baudin, F., Bout-Roumazeilles, V., and Lyons, T.W., 2011, Unexpectedly low organic matter content in Cariaco Basin sediments during the Younger Dryas: Origin and implications: Comptes Rendus Geoscience, v. 343, p. 351-359.

Saenger, A., Cécillon, L., Sebag, D., and Brun, J., 2013, Soil organic carbon quantity, chemistry and thermal stability in a mountainous landscape: a Rock–Eval pyrolysis survey: Organic Geochemistry, v. 54, p. 101-114.

Sanei, H., Stasiuk, L., and Goodarzi, F., 2005, Petrological changes occurring in organic matter from recent lacustrine sediments during thermal alteration by Rock-Eval pyrolysis: Organic Geochemistry, v. 36, p. 1190-1203.

Sapkota, A., Krachler, M., Scholz, C., Cheburkin, A.K., and Shotyk, W., 2005, Analytical procedures for the determination of selected major (Al, Ca, Fe, K, Mg, Na, and Ti) and trace (Li, Mn, Sr, and Zn) elements in peat and plant samples using inductively coupled plasma-optical emission spectrometry: Analytica Chimica Acta, v. 540, p. 247-256.

Sebag, D., Disnar, J., Guillet, B., Di Giovanni, C., Verrecchia, E.P., and Durand, A., 2006, Monitoring organic matter dynamics in soil profiles by 'Rock-Eval pyrolysis': bulk characterization and quantification of degradation: European Journal of Soil Science, v. 57, p. 344-355.

Steinmann, P., Adatte, T., and Lambert, P., 2003, Recent changes in sedimentary organic matter from Lake Neuchatel (Switzerland) as traced by Rock-Eval pyrolysis, *in* Lake Systems from the Ice Age to Industrial Time: Springer, p. 109-116.

Tamburini, F., Adatte, T., Föllmi, K., Bernasconi, S.M., and Steinmann, P., 2003, Investigating the history of East Asian monsoon and climate during the last glacial–interglacial period (0–140 000 years): mineralogy and geochemistry of ODP Sites 1143 and 1144, South China Sea: Marine Geology, v. 201, p. 147-168.

Thompson, R., Battarbee, R., O'Sulliuan, P., and Oldfield, F., 1975, Magnetic susceptibility of lake sediments: Limnology, .

Tingstad, A., Moser, K.A., MacDonald, G.M., and Munroe, J.S., 2011, A~ 13,000-year paleolimnological record from the Uinta Mountains, Utah, inferred from diatoms and loss-on-ignition analysis: Quaternary International, v. 235, p. 48-56.

Tribovillard, N., Bout-Roumazeilles, V., Algeo, T., Lyons, T.W., Sionneau, T., Montero-Serrano, J.C., Riboulleau, A., and Baudin, F., 2008, Paleodepositional conditions in the Orca Basin as inferred from organic matter and trace metal contents: Marine Geology, v. 254, p. 62-72.

Tribovillard, N., Bout-Roumazeilles, V., Sionneau, T., Serrano, J.C.M., Riboulleau, A., and Baudin, F., 2009, Does a strong pycnocline impact organic-matter preservation and

accumulation in an anoxic setting? The case of the Orca Basin, Gulf of Mexico: Comptes Rendus Geoscience, v. 341, p. 1-9.

Untermann, G., and Untermann, B., 1969, Geology of the Uinta Mountain area, Utah-Colorado: .

Van Der Putten, N., Hébrard, J., Verbruggen, C., Van de Vijver, B., Disnar, J., Spassov, S., De Beaulieu, J., De Dapper, M., Kéravis, D., and Hus, J., 2008, An integrated palaeoenvironmental investigation of a 6200 year old peat sequence from Ile de la Possession, Iles Crozet, sub-Antarctica: Palaeogeography, Palaeoclimatology, Palaeoecology, v. 270, p. 179-195.

Vierling, L.A., 1998, Palynological evidence for late-and postglacial environmental change in central Colorado: Quaternary Research, v. 49, p. 222-232.

Whiteman, C.D., 2000, Mountain meteorology: fundamentals and applications: Oxford University Press, .

Wolyn, P.G., and McKee, T.B., 1989, Deep stable layers in the intermountain western United States: Monthly Weather Review, v. 117, p. 461-472.

Zocatelli, R., Turcq, B., Boussafir, M., Cordeiro, R.C., Disnar, J., Costa, R., Sifeddine, A., Albuquerque, A.L.S., Bernardes, M., and Jacob, J., 2012, Late Holocene paleoenvironmental changes in Northeast Brazil recorded by organic matter in lacustrine sediments of Lake Boqueirão: Palaeogeography, Palaeoclimatology, Palaeoecology, v. 363, p. 127-134.

Appendix I

Core Log

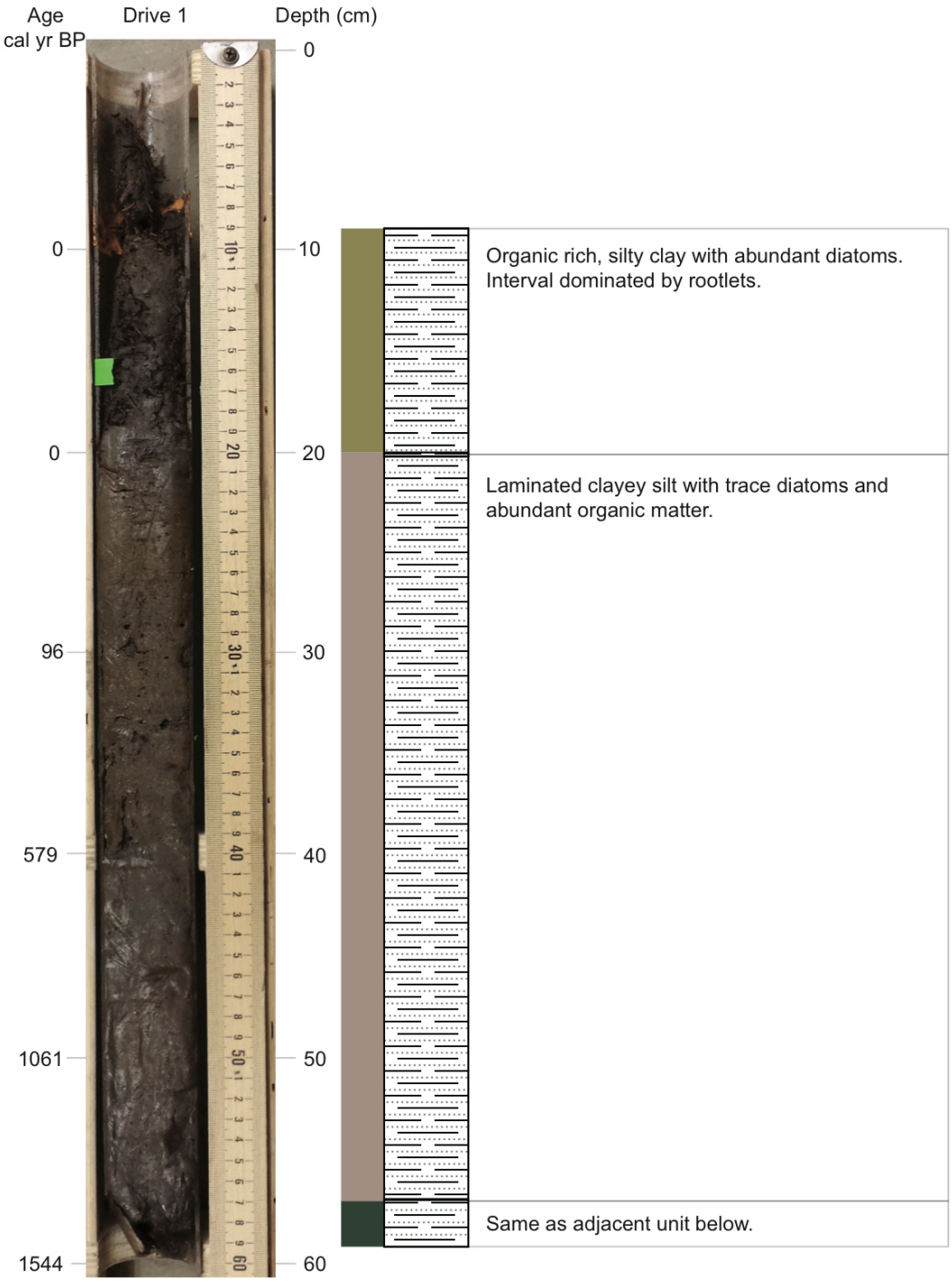

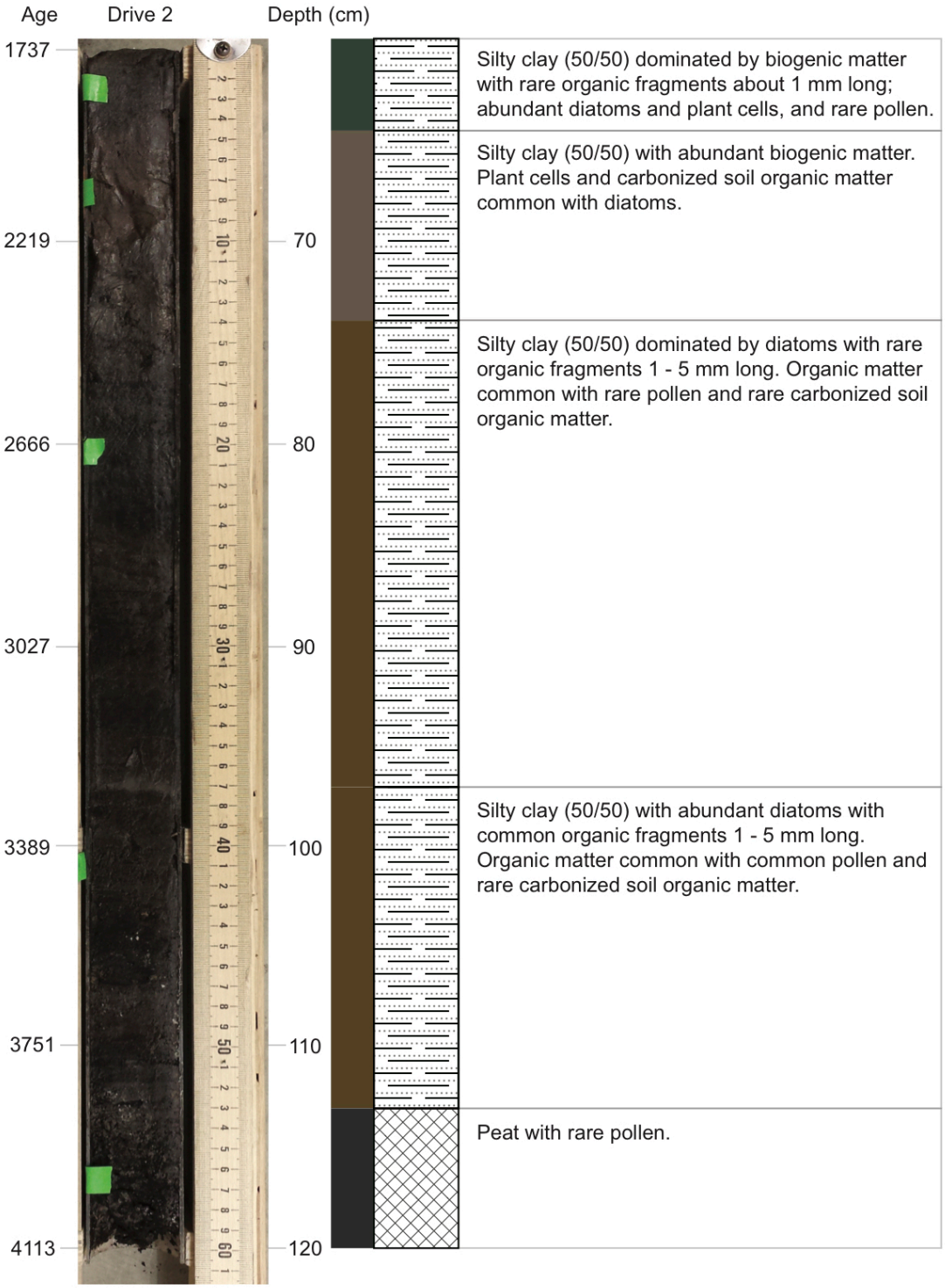
Age
Drive 2
Depth (cm)
1737
2219
2666
3027
3389
3751
4113
70
80
90
100
110
120
Silty clay (50/50) dominated by biogenic matter with rare organic fragments about 1 mm long; abundant diatoms and plant cells, and rare pollen.
Silty clay (50/50) with abundant biogenic matter. Plant cells and carbonized soil organic matter common with diatoms.
Silty clay (50/50) dominated by diatoms with rare organic fragments 1 - 5 mm long. Organic matter common with rare pollen and rare carbonized soil organic matter.
Silty clay (50/50) with abundant diatoms with common organic fragments 1 - 5 mm long. Organic matter common with common pollen and rare carbonized soil organic matter.
Peat with rare pollen.

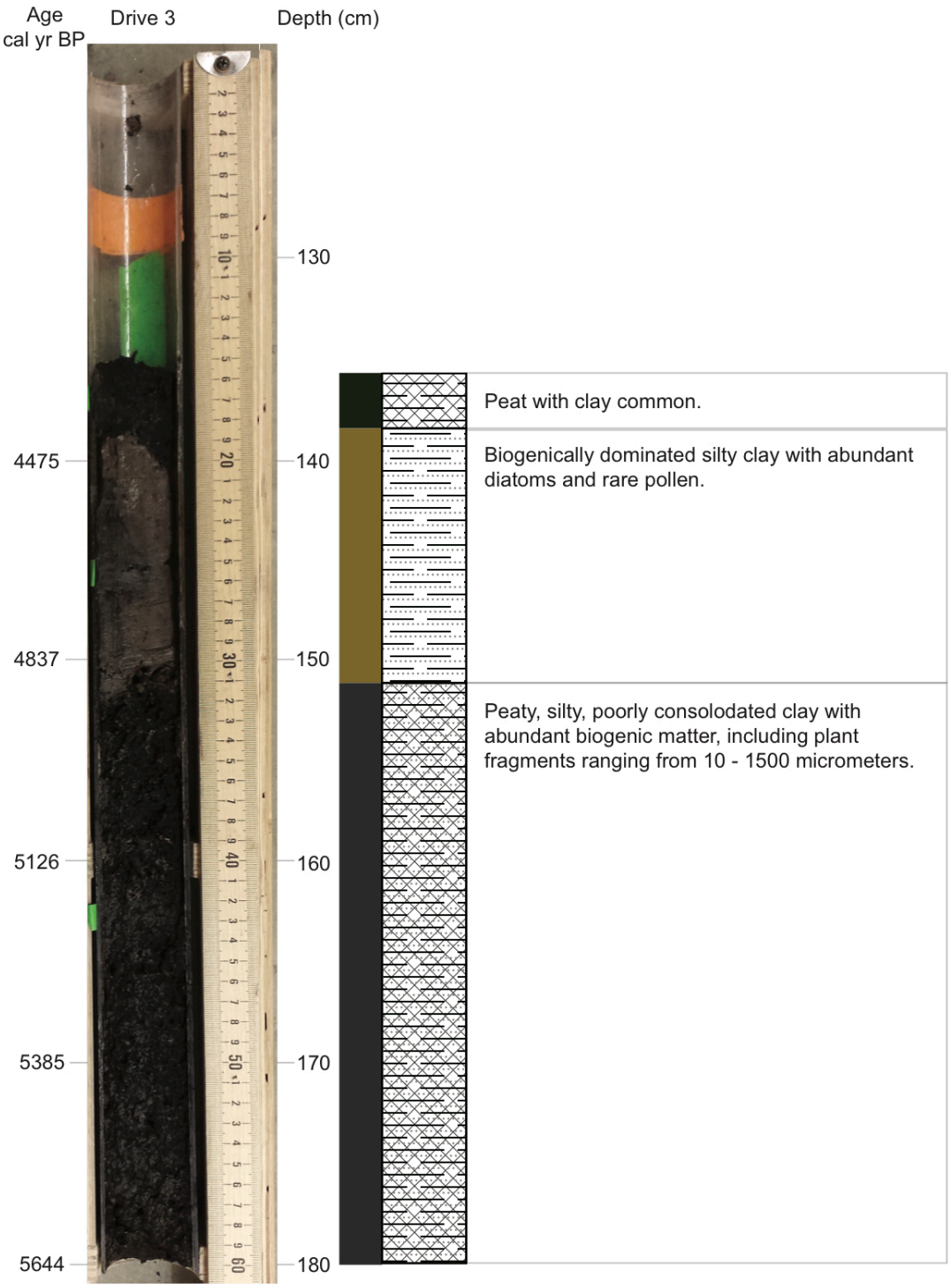
Age
cal yr BP
Drive 3
Depth (cm)
4475
4837
5126
5385
5644
130
140
150
160
170
180
Peat with clay common.
Biogenically dominated silty clay with abundant diatoms and rare pollen.
Peaty, silty, poorly consolodated clay with abundant biogenic matter, including plant fragments ranging from 10 - 1500 micrometers.

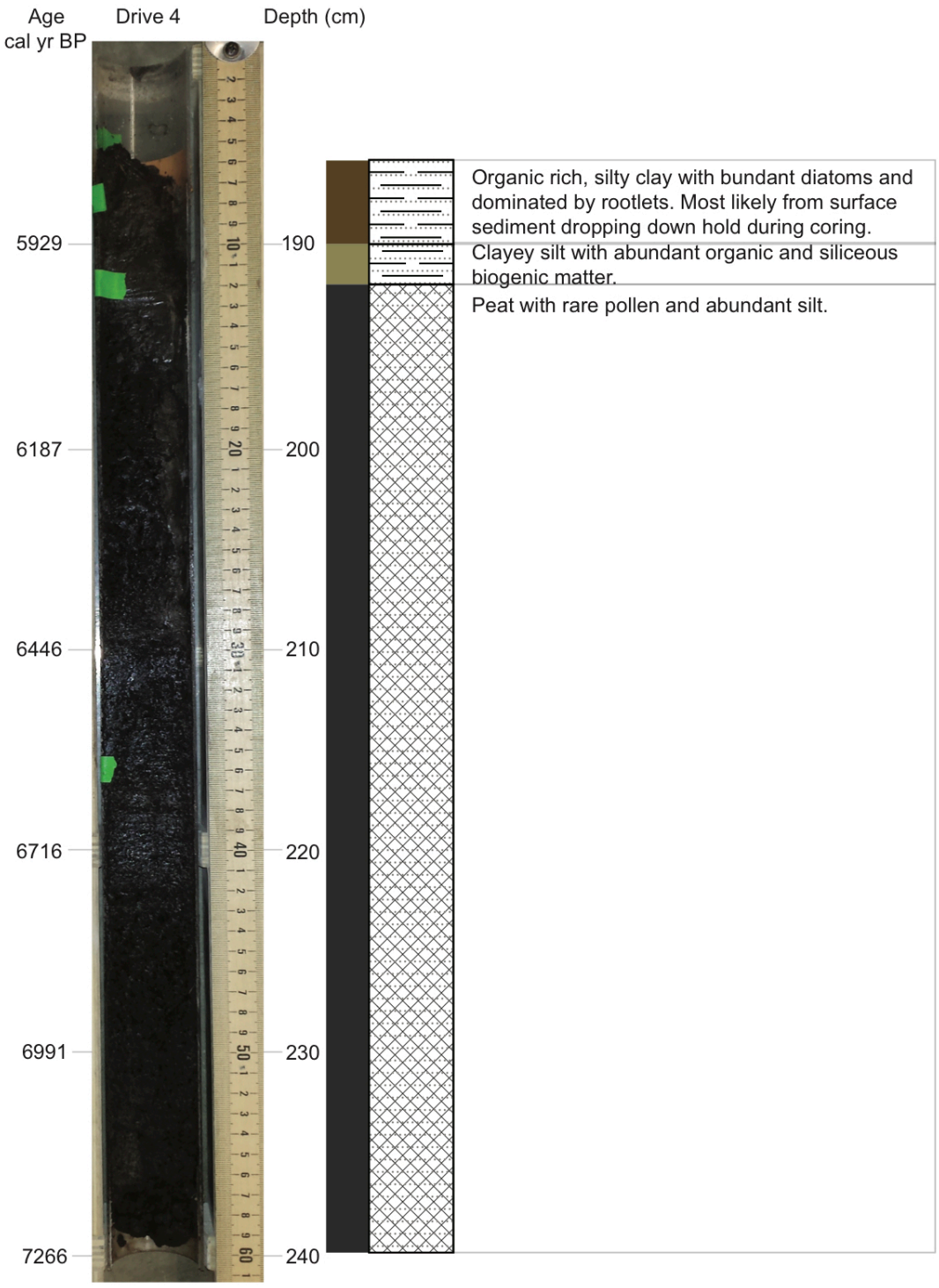
Age
cal yr BP
Drive 4
Depth (cm)
5929
6187
6446
6716
6991
7266
190
200
210
220
230
240
Organic rich, silty clay with bundant diatoms and dominated by rootlets. Most likely from surface sediment dropping down hold during coring.
Clayey silt with abundant organic and siliceous biogenic matter.
Peat with rare pollen and abundant silt.

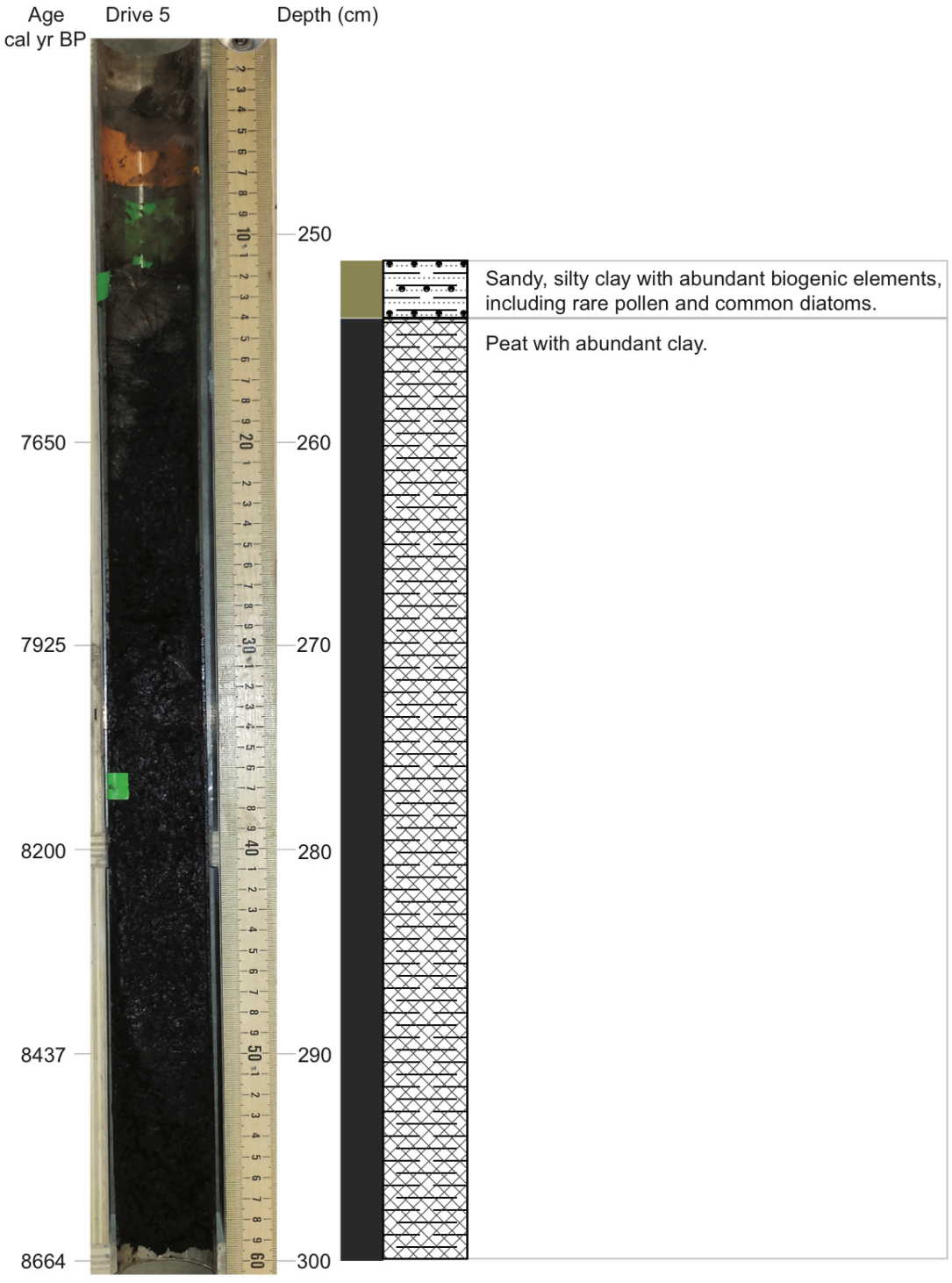
Age
cal yr BP
Drive 5
Depth (cm)
7650
7925
8200
8437
8664
250
260
270
280
290
300
Sandy, silty clay with abundant biogenic elements, including rare pollen and common diatoms.
Peat with abundant clay.

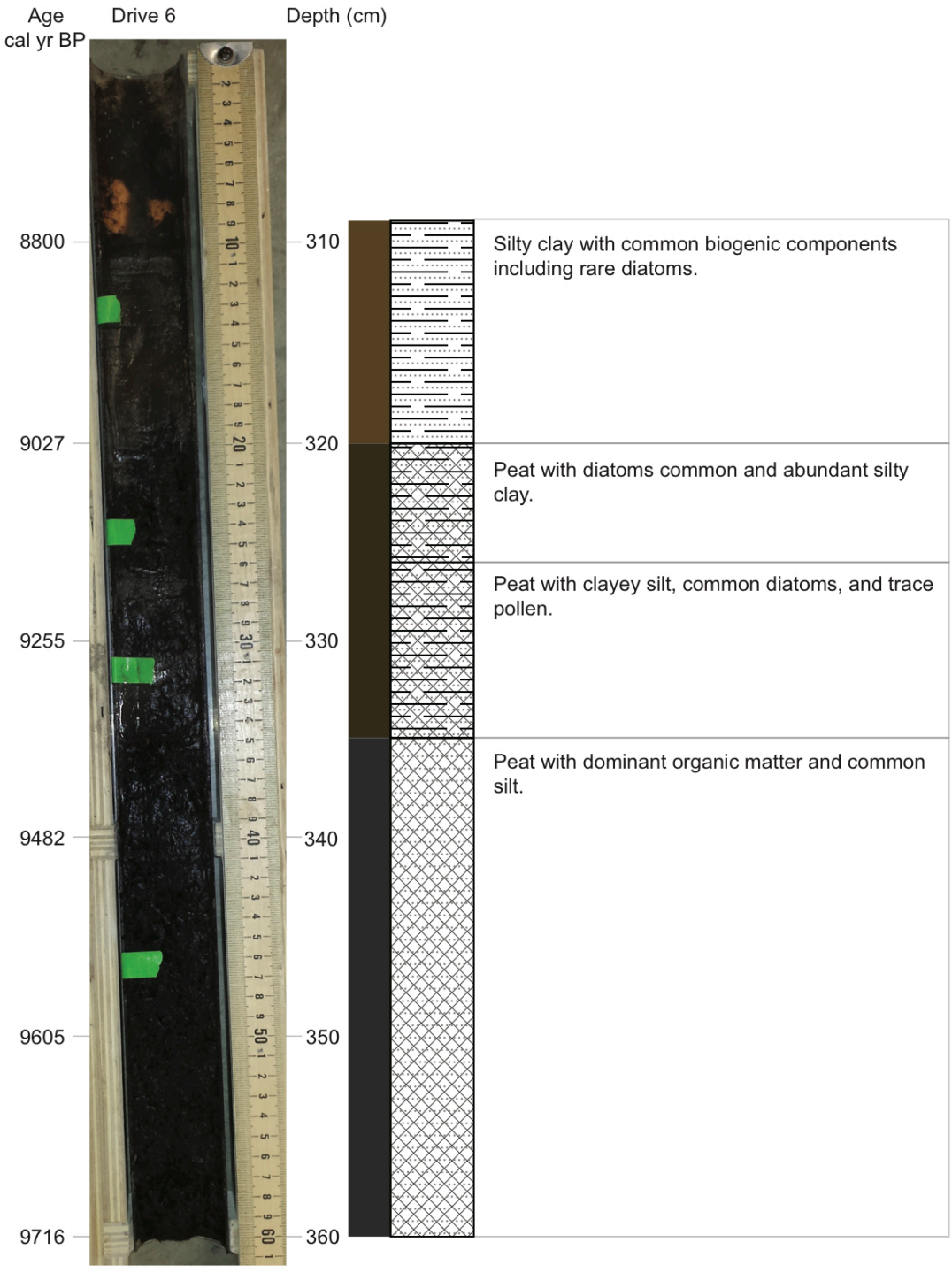
Age
cal yr BP
Drive 6
Depth (cm)
8800
9027
9255
9482
9605
9716
310
320
330
340
350
360
Silty clay with common biogenic components including rare diatoms.
Peat with diatoms common and abundant silty clay.
Peat with clayey silt, common diatoms, and trace pollen.
Peat with dominant organic matter and common silt.

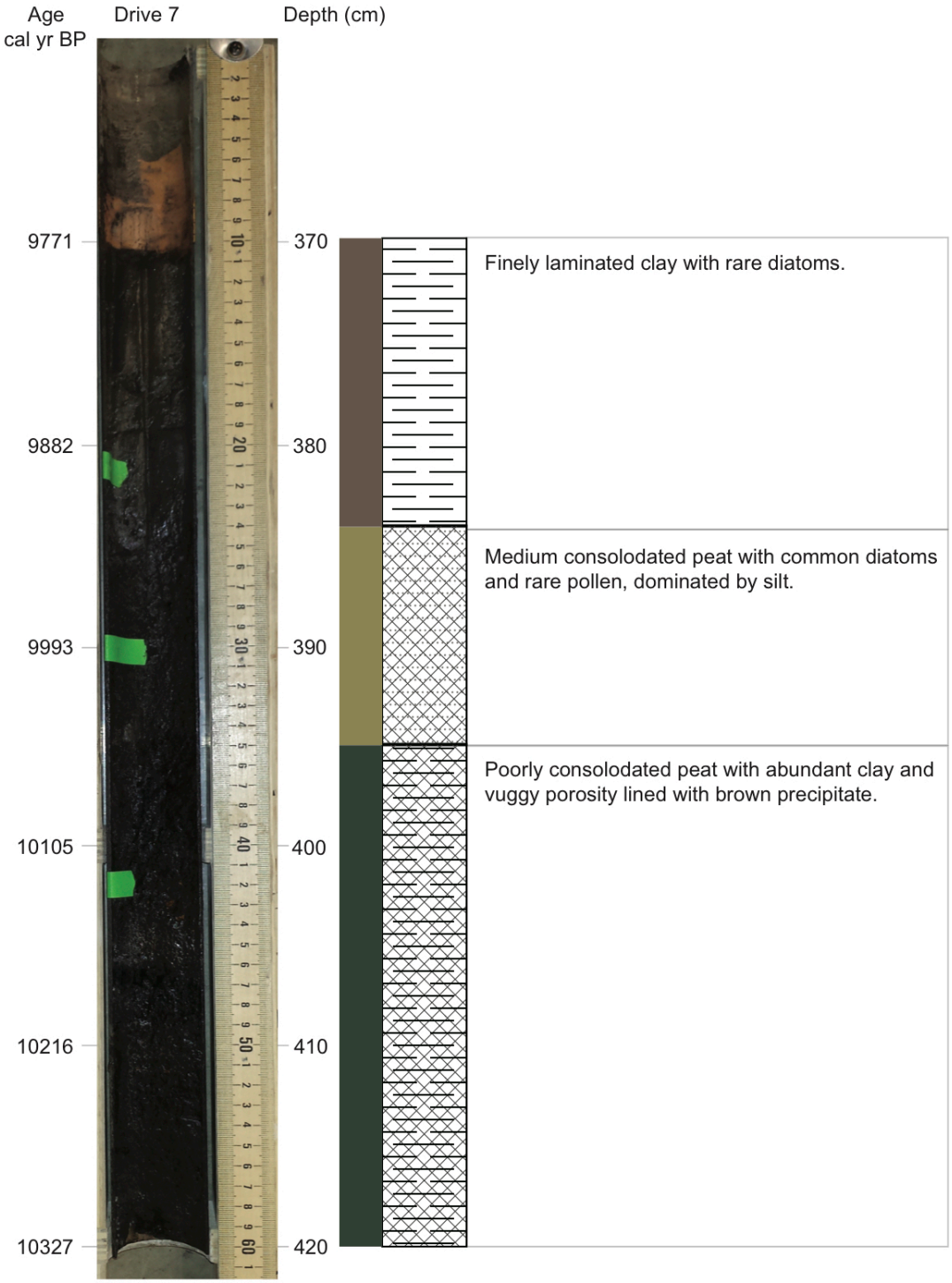
Age
cal yr BP
Drive 7
Depth (cm)
9771
9882
9993
10105
10216
10327
370
380
390
400
410
420
Finely laminated clay with rare diatoms.
Medium consolodated peat with common diatoms and rare pollen, dominated by silt.
Poorly consolodated peat with abundant clay and vuggy porosity lined with brown precipitate.

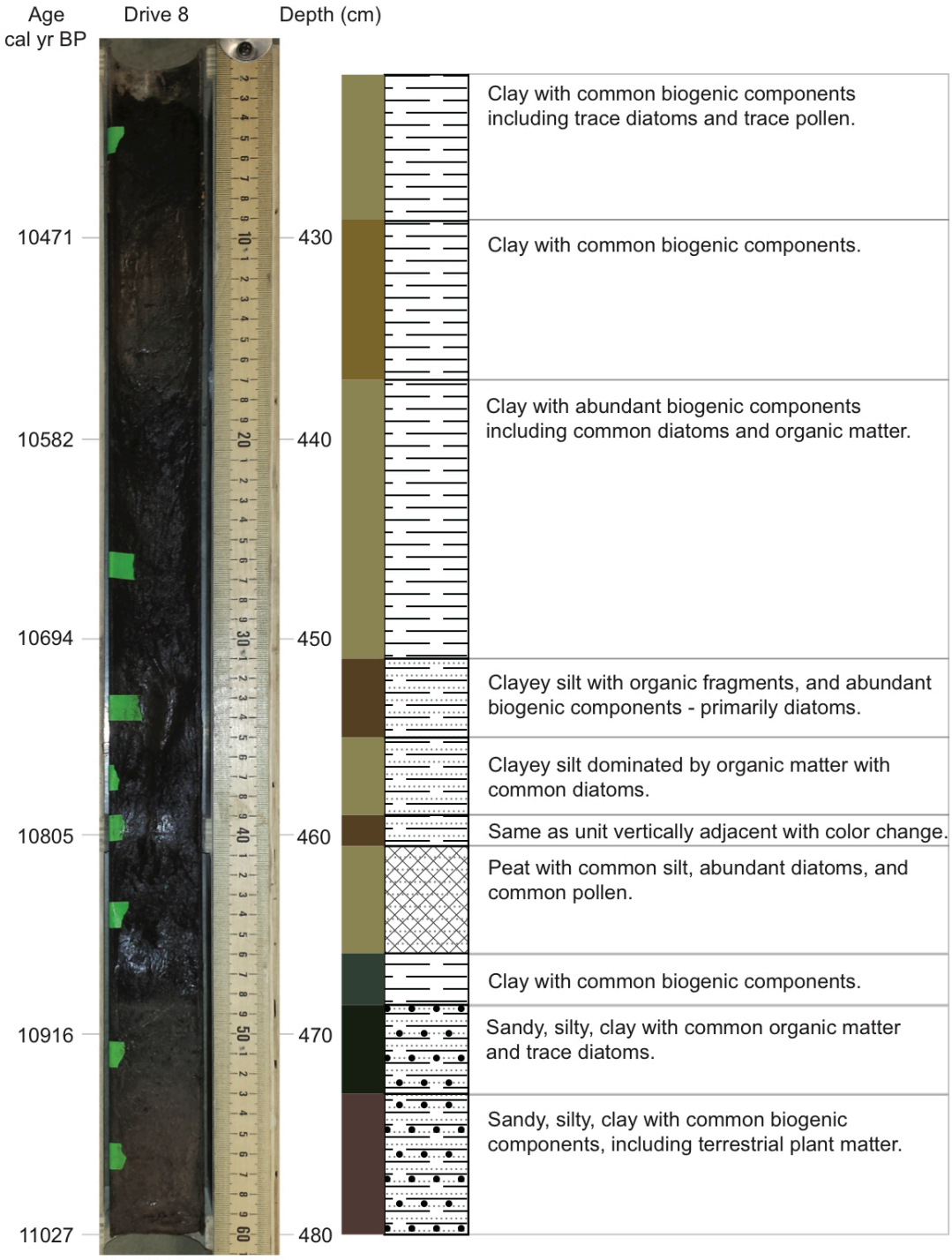
Age
cal yr BP
Drive 8
Depth (cm)
10471
10582
10694
10805
10916
11027
430
440
450
460
470
480
Clay with common biogenic components including trace diatoms and trace pollen.
Clay with common biogenic components.
Clay with abundant biogenic components including common diatoms and organic matter.
Clayey silt with organic fragments, and abundant biogenic components - primarily diatoms.
Clayey silt dominated by organic matter with common diatoms.
Same as unit vertically adjacent with color change.
Peat with common silt, abundant diatoms, and common pollen.
Clay with common biogenic components.
Sandy, silty, clay with common organic matter and trace diatoms.
Sandy, silty, clay with common biogenic components, including terrestrial plant matter.

Figure 4: Core log with descriptions from microscopic and macroscopic observations. Definitions: dominant >50%, abundant 25 - 50%, common 5 - 25%, rare 1 - 5%, trace <1%. From left to right: age cal yr BP (1950); core image with green tape marking smear slide locations; core depth; color log based on Munsell color chart; lithologic log - represented by combination of lithologies pictured above; and core description.

Appendix II

Trace Element Dust as Climate Indicator

Atmospheric dust fluxes may increase with drier conditions. Lambert et al. (2008) noted a 25-fold increase in windblown dust across 8 ice ages in the past 800,000 years. They attribute the increase in dust flux to strengthened dust sources and reduced hydrological cycles. Mahowald et al. (1999) link decreased vegetation at higher altitudes to increased dust sources. Drier conditions would act as a catalyst to decreased vegetation and an increase in dust fluxes. If trace element dust could be isolated in the core samples of this study, the data could be used to further identify the dry periods.

Methods

Inductively Coupled Plasma-Optical Emission Spectrometry (ICP-OES) Trace Element Dust Analysis

Remaining sample from pyrolysis preparation was used. For intervals lacking at least 200 mg, more sample was prepared. Resampled intervals were primarily peat and required use of the archived core. If the archived half had sufficient material, it was sampled by itself. If it lacked enough material, sediment was taken from both core halves. The same collection processes were followed. Open samples vials were placed into a 60 °C oven overnight and removed and capped when dry.

Sample Fusion, Digestion, and Dilution

Dry samples were fused with lithium tetraborate and a wetting agent, then digested in concentrated trace metal grade nitric acid. Methods similarly follow R.W., Murray et al. (2000).

Platinum crucibles were acid washed in 20% HCl on a hotplate for 20 minutes, then triple rinsed with Milli Q water and oven dried. Once dried, crucibles were removed from the oven and covered with Parafilm wax to prevent dust contamination (samples were continually capped with Parafilm when not in use). Crucibles were numbered with a heat resistant marker sufficient to withstand over 1050 °C to track samples. 10 mL centrifuge tubes were triple rinsed with 10% HCl, then rinsed with Milli Q water and air dried in a laminar flow hood.

For fusion, crucibles were transported to a four-decimal place balance. Individual crucibles were tared on the balance and sample was added directly with a clean stainless steel spatula. An approximate ratio of 1:4 sample to flux was added and true masses of both flux and sample recorded. Between 0.2000 and 0.2500 grams of sediment sample was carefully added to the crucible, the mass was recorded and the balanced tared. Between 0.8000 and 0.9000 grams of lithium metaborate flux containing a non-wetting agent were then added to the crucible and the mass recorded. The sediment and flux were homogenized by gently turning and shaking the crucible. When combined, the crucible was tilted and gently tapped with finger or on a wood surface to isolate sample on one side. Because the sample shrinks when fused, keeping sediment isolated helped create one coherent fused mass.

Crucibles were taken to a high temperature muffle furnace, uncovered and placed into the oven, which was previously warmed to 300 °C. The oven temperature was then set to 1000 °C. When at temperature, samples were given at least 15 minutes to completely fuse.

The crucibles were removed and set to cool on a ceramic plate. Visually inspecting each fusion was necessary to ensure all flux and sediment had fused, as well as coherence of fused sample. If fusion was incomplete it was returned to the oven for another 15 minutes before removing and inspecting again. To release the glass, the crucibles were capped with Parafilm and gently tapped on wood until the sample was dislodged.

Crucibles were gently tapped on wood to loosen bead fusion. Samples were taken to the balance where a 10 mL centrifuge tube had been tared. A crucible was carefully tilted to allow the bead to slide into the centrifuge tube for measurement. Measured samples were capped, labeled and placed in a gallon size freezer Ziploc bag.

A blank was prepared roughly every 15 samples to help identify contaminants in preparation. The blank underwent the same preparation as typical samples except that sediment was excluded from the mixture when added to the crucible.

Ziploc bags carrying samples were placed in a laminar flow hood where centrifuge tubes were removed and placed in stands vertically. With nitrile gloves caps were carefully removed, and a 10 mL pipette was used to add 5 mg trace metal grade, concentrated nitric acid to each

tube. Tubes were oriented horizontally and continually mixed on a shaker table at 215 RPM for 24 hours to digest.

Digestion seemed incomplete because the flux super-saturated the acid and formed precipitate. Topping off the samples with Milli-Q deionized water showed dilution effective to greater digestion. So, samples were transferred to larger centrifuge tubes, water added, and vials shaken.

Samples were transferred under a Hepa filtered flow hood to 50 mL centrifuge tubes that had been acid washed, labeled, and weighed. 10 mL sample tubes were poured directly into new vials. Milli-Q deionized water was then added to each 10 mL sample tube until ½ to ¾ full. The tube was capped and shaken and the solution poured into the new 50 mL centrifuge tube. This process was repeated at least three times until all the sample was transferred, and the 50 mL tubes topped with the water.

Now full, the new sample vials were placed in an oven at 60 °C to warm the acid and stimulate reactions. Once warmed (2 hours for good measure), the samples were oriented horizontally and placed on a shaker table at 100 RPM for 72 hours.

Each sample was then spun at ~2900 RPM for 5 minutes to separate remaining solid precipitate. The sample weight was recorded and subtracted from the original dry weight of the centrifuge tube and taken for analysis on the ICP-OES where solution water was extracted directly from the vial.

Further Digestion and Dilution

Despite best efforts, precipitate persisted in each diluted 50mL sample centrifuge tube. The supernatant was decanted from each and the uncapped centrifuge tubes were desiccated overnight in the SuperModulyo Freeze dryer. Dried samples were recapped with their original tops and their weights recorded. 2 drops of concentrated hydrofluoric acid (HF) and 1 mL of Milli Q deionized water were added to remaining precipitate in each sample tube and left overnight to react. 2 additional drops of HF were added and the samples placed in an oven at 60 °C for 48 hours to foster digestion. Any additional HF for digestion could not be diluted sufficiently in the 50 mL centrifuge tubes to not damage the ICP-OES. Sample tubes were then filled between 45 and 50 mL with Milli Q water, weights were recorded, and samples hand shaken for 3-5 seconds and oriented vertically in a holding tray. 24 hours later, samples were all spun at 3200 RPM for 5 minutes and placed again vertically in centrifuge tray. The diluted samples were again analyzed in the ICP-OES.

Again, some precipitate persisted. It seems reasonable that the same methods could be repeated to try and ascertain the amount and percentage of trace elements in the remaining precipitates, though the question of dilution beyond detectable limits arrives eventually. Continued handling also raises the question of sample integrity.

Landslide Detritus Analysis

Average maximum mineral grain sizes of the most clastic rich core intervals were measured using the previously prepared smear slides (Myrbo, 2013). Four smear slides were selected for measurement using the lithologic log as a reference. Slides from drive 2, 4, 5, and 8 were used. The average large mineral size from drive 4 was 200 microns; the average from drive 5 was 100 microns; and the average for drives 2 and 8 was 50 microns. Sediment collect from the landslide was then passed through 80 mesh (177 microns). 80 mesh was used because it is closer to the mean of the averages and more representative of the grain size the energy in the system would wash in, while including some of the larger potential clasts.

Sediment was then fused, prepared for ICP-OES analysis, and analyzed in the same manner as all previous samples, except the flux to sediment ratio during fusion was ~ 2:1, instead of ~4:1. Because this sediment was clastic, the standard 2:1 ratio (Ingamells, 1970) was used and proved more effective for removing the fusion from the crucible and for acid digestion.

Fen Water Collection and Analysis

A borehole was hand augured until refusal by cobbles. Assuming that to be the bottom of the fen, approximately 4.9 m deep, we installed a piezometer with traditional sand and gravel at the base, and bentonite clay above. Several purging attempts were made, though slow recharge from high clay content only permitted one purge before water sample collection.

This first well was destroyed, likely by cattle, so a second was hand augured. Its location is likely closer to the fen depocenter. Water flowed at 1.2 m and 4.3 m. At 4.3 m the thick peat

layers started to collapse in on itself. 4.3 m was isolated for the new water interval to sample from. This well produced water nearly to the surface and was purged 4 times before samples were collected.

The final purging was completed 2 hours before sampling, and fortuitously, this time the water at depth ran clear. It was pumped through acid washed hoses, fed through a 4.5 micron filter and directly into an acid washed bottle. Three drops of nitric acid were added to prevent partitioning trace elements into the mineral and losing some of the water's natural fingerprint. A second water sample was taken as before, though without the 4.5 micron filter. This time, an acid washed 200 Mesh (74 micron) screen was used at the hose tip. The water was refrigerated until ICP-OES analysis when water was taken directly from the sample bottle.

Dust Differentiation

To isolate the dust flux signal from washed in elements the sieved landslide detritus composition was to be compared with the *in situ* water composition. Elements in excess of detrital concentrations were assumed to represent windblown dust. Dust fluxes were to be identified in the core with spikes in those elements.

Results

Samples never completely digested, leaving the ICP-OES results compromised and deemed unsuitable for trace element analysis. Collected fen water samples were analyzed and are

considered valid. Though not used as intended for comparison against sediment analysis, fen water ICP-OES results may be useful in another study.

Appendix III

Correlation Table for Figure 7 data

	Lithology	*Mag Susc*	*HI*	*Biomass /TOC*
Lithology	1			
Mag Susc	-0.368	1		
HI	0.648	-0.590	1	
Biomass/TOC	0.718	-0.559	0.838	1

Appendix IV

ICP Data as Measured

	mg/L	ppm	ppm	mg/L	ppm	mg/L	mg/L	mg/L	mg/L	mg/L	mg/L	mg/L	ppm	ppm	mg/L	mg/L	mg/L	mg/L	mg/L	mg/L	ppm	ppm
Sample	Al1670	As1937	B_2496	Ba4554	Ca3158	Fe2599	K_7664	Li6707	Mg2795	Mn2576	Mo2020	Na5895	P_1774	Pb2203	Sb2068	Se1960	Si2516	Sr4077	Tl1908	V_2924	Zn2138
6	76.16	0.2246	2507	2.507	18.13	181.5	87.01	437.8	13.87	10.83	0.0124	37.02	3.918	0.1895	-0.027	-0.13	61.09	0.3161	-0.0168	0.2981	0.2047
9	68.24	-0.0305	2701	2.028	40.75	83.86	67.9	422	16.62	0.7541	0.0143	31.28	4.543	0.3825	-0.028	-0.1089	158.2	0.3731	-0.0221	0.2468	0.285
10	65.51	0.025	2742	2.339	32.84	96.1	65.14	429.7	15.09	1.304	0.0137	31.48	4.182	0.2306	-0.0279	-0.1149	94.5	0.3428	-0.0216	0.2572	0.2094
11	69.42	-0.0904	2710	4.064	49.57	94.16	60.46	422.3	20.69	0.3964	0.0105	26.95	5.045	0.1684	-0.0274	-0.1131	56.1	0.4923	-0.0253	0.3709	0.2072

14	70.83	-0.0926	2641	3.303	34.86	122.2	91.97	423.7	21.42	1.074	0.0102	40.72	4.254	0.1855	-0.0231	-0.1205	60.72	0.4592	-0.0273	0.3474	0.252
15	66.38	-0.0731	2696	3.571	36.14	84.16	76.55	435.9	18.54	0.5925	0.0116	46.3	4.13	0.1385	-0.0263	-0.1079	41.9	0.4911	-0.023	0.3143	0.1834
16	76.74	-0.1031	2522	2.289	31.04	75.68	82.47	432.3	16.94	1.373	0.0133	30.41	9.623	0.3011	-0.0275	-0.1112	103.1	0.4021	-0.0235	0.2719	0.2836
17	69.34	-0.0197	2474	2.432	42.69	72.74	37.79	460.5	12.71	0.4628	0.0173	8.864	4.082	0.1417	-0.0265	-0.1041	46.22	0.2221	-0.0146	0.1636	0.1579
18	67.59	-0.043	2793	3.962	39.75	139.8	106	432.3	27.43	0.9471	0.0098	42.79	4.565	0.1841	-0.0232	-0.1177	61.19	0.5451	-0.0279	0.3732	0.3092
19	66.79	0.0865	2717	3.259	33.83	136.5	73.34	418.6	18.23	1.22	0.0123	31.75	4.519	0.2289	-0.0237	-0.1201	96.56	0.4213	-0.0267	0.3239	0.2187

20	72.6	0.0348	2480	1.931	34.97	46.87	43.9	431.3	10.88	0.4049	0.0174	21.98	4.158	0.2239	-0.0293	-0.1075	81.78	0.2869	-0.0178	0.1713	0.1327
21	30.7	-0.0598	3135	3.269	38.3	93.66	59.06	^**** *	22.06	0.979	0.0101	14.51	2.995	0.2303	-0.0217	-0.1025	90.98	0.3892	-0.0275	0.3388	0.2095
22	24.43	0.0766	3227	1.289	38.81	39.55	10.32	^**** *	5.751	0.3208	0.0196	13.55	2.76	0.0979	-0.032	-0.1045	27.3	0.1879	-0.0102	0.0784	0.0435
23	0.3688	-0.0047	3186	0.0017	0.0676	0.3435	0.5817	463.7	0.0378	0.0044	0.0119	4.109	0.0478	0.0429	-0.0345	-0.1019	-5.473	0.0015	-0.0075	0.0013	0.0022
24	32.06	0.0166	3147	4.153	37.56	113.9	64.7	^**** *	25.37	1.237	0.0116	10.39	3.119	0.2472	-0.0206	-0.1068	98.6	0.3137	-0.028	0.3748	0.3337
25	72.55	-0.0105	2665	2.121	32.25	107.2	83.95	420.6	25.67	0.5152	0.0135	11.15	3.704	0.2547	-0.0235	-0.1119	107.2	0.2495	-0.0223	0.3115	0.247

26	0.2295	0.0166	2940	0.0014	0.0307	0.6905	0.87	421.6	0.0083	0.0011	0.01	2.52	0.0536	0.0432	-0.033	-0.1017	-5.306	0.001	-0.0067	0.0024	0.002
27	41.21	0.0944	3101	3.217	38.77	124.1	74.12	^**** *	25.01	0.645	0.0139	19.74	3.178	0.3646	-0.0266	-0.1153	162.8	0.3134	-0.0214	0.327	0.3831
28	48.87	0.0925	3023	2.576	31.04	166.3	76.83	444	17.18	1.567	0.0117	37.47	3.726	0.2841	-0.0258	-0.1253	123.5	0.3905	-0.0271	0.3302	0.2234
29	0.3715	0.0314	2798	0.0018	0.0518	0.1899	0.6263	414.2	0.0129	0.0007	0.0095	2.414	0.0537	0.0423	-0.0336	-0.0962	-5.037	0.0012	-0.0066	0.0012	0.0024
30	50.76	0.0262	3049	3.628	41.5	156.3	79.24	436.7	20.39	1.889	0.0143	37.93	4.806	0.2033	-0.0269	-0.1257	77.74	0.4651	-0.0257	0.3555	0.2683
31	64.96	-0.0926	2786	5.527	34.27	77.71	92.75	433	20.76	0.5118	0.01	68.65	2.305	0.2388	-0.0242	-0.1053	94.72	0.6488	-0.0276	0.2725	0.2529

32	73.24	0.0443	2561	2.469	22.62	134.9	87.98	422.2	16.35	1.865	0.0108	38.11	3.805	0.1381	-0.026	-0.1172	37.08	0.3535	-0.0239	0.2878	0.2352
33	65.34	0.1196	2307	1.111	32.4	26.11	18.63	430.4	5.458	0.3475	0.019	14.24	4.215	0.123	-0.0318	-0.1033	31.85	0.2019	-0.0132	0.0793	0.062
34	63.6	-0.0396	2943	4.742	60.58	99.41	57.95	428.3	19.41	0.3424	0.0106	32.68	5.815	0.2533	-0.0296	-0.1145	103.4	0.5704	-0.0269	0.4308	0.1927
35	77.42	-0.0345	2405	2.076	9.532	60.13	93.87	424.3	12.27	0.2305	0.0122	43.2	2.033	0.381	-0.0295	-0.1043	141.2	0.2492	-0.0224	0.2212	0.1442
36	54.29	-0.1043	2919	4.096	47.02	95.15	69.42	453.5	22.82	0.6187	0.0102	31.48	4.996	0.2166	-0.0277	-0.1137	86.55	0.5029	-0.0238	0.3531	0.2022
37	63.65	0.0334	2658	1.427	38.9	42.38	36.08	434	10.09	0.4479	0.022	17.2	4.724	0.1485	-0.029	-0.0992	52.75	0.2564	-0.0129	0.1292	0.1073

38	81.01	-0.0452	2339	2.571	34.98	70.43	74.65	427	16.09	0.3346	0.0187	23.35	4.416	0.1775	-0.0279	-0.1125	54.86	0.4121	-0.0223	0.2311	0.221
39	80.92	-0.0382	1763	2.806	40.82	88.11	61.35	386.9	18.6	0.4792	0.0137	7.248	4.565	0.2044	-0.0189	-0.0904	75.92	0.228	-0.0189	0.231	0.1774
40	50.17	0.0713	2947	2.282	75.63	77.07	16.31	439.3	8.783	0.3019	0.0127	13.48	3.719	0.1228	-0.027	-0.1069	36.26	0.4081	-0.0165	0.3085	0.0876
41	64.72	0.0297	2707	1.724	31.04	54.89	42.38	421.3	11.28	0.633	0.016	29.25	4.476	0.2625	-0.0295	-0.1082	107.7	0.2844	-0.0162	0.1367	0.1954
42	56.37	0.2263	2860	2.396	20.72	175	89.29	455.9	16.08	3.487	0.0121	40.14	3.938	0.2161	-0.0261	-0.1192	86.87	0.3551	-0.0239	0.3482	0.2103
43	85.99	0.1386	2239	3.431	37.35	107	86.69	419.2	21.64	0.4094	0.0154	9.707	4.228	0.2284	-0.0256	-0.1203	73.93	0.2732	-0.0259	0.365	0.4329

45	60.14	0.0041	2938	2.909	33.95	133.4	79.7	440.8	18.34	1.074	0.0106	38.92	4.064	0.2304	-0.0256	-0.1208	92.86	0.4119	-0.0259	0.3332	0.2339
46	70.61	0.052	2734	3.14	15.33	141.7	87.21	422.6	12.41	1.642	0.0119	36.24	2.84	0.2028	-0.0286	-0.1203	72.69	0.2937	-0.0221	0.242	0.1785
47	82.01	0.3331	2783	3.116	26.38	209.9	114.9	438	18.97	2.903	0.0155	54.65	6.913	0.2636	-0.0323	-0.161	81.43	0.4424	-0.0371	0.4112	0.3403
48	59.48	0.0355	2466	1.678	50.56	46.59	17.55	425.4	7.287	0.5263	0.0135	13.85	4.128	0.1056	-0.0284	-0.0993	30.74	0.2726	-0.0128	0.0737	0.104
49	65.27	-0.1037	2917	3.721	43.83	80.13	54.88	428.4	20.77	0.3428	0.0116	28.1	4.689	0.2467	-0.0293	-0.1158	104.3	0.4592	-0.0226	0.3096	0.1768
50	78.77	-0.029	2239	2.663	35.94	65.36	65.04	413.2	14.66	0.5017	0.0138	38.98	5.666	0.2161	-0.0282	-0.1093	69.48	0.3685	-0.0209	0.1641	0.5521

51	64.12	0.0889	2119	1.359	36.36	36.85	18.89	404.6	6.631	0.2993	0.0153	11.76	3.889	0.1245	-0.0236	-0.0885	40.33	0.1934	-0.0123	0.0922	0.0634
52	75.05	0.0143	1395	1.062	22.33	41.58	29.41	345.9	7.044	0.2819	0.0086	13.89	2.646	0.1494	-0.0166	-0.0668	51.61	0.1898	-0.013	0.1408	0.1094
53	38.09	0.2482	3185	2.723	39.42	148.8	58.3	472.2	16.29	1.87	0.015	30.76	4.286	0.1603	-0.0273	-0.1234	54.38	0.3947	-0.0223	0.3132	0.2228
54	62.39	-0.0663	2811	3.491	53.23	88.88	44.8	419.6	16.63	0.2964	0.0104	20.71	5.48	0.1375	-0.0273	-0.1104	41.16	0.442	-0.0205	0.3468	0.147
55	0.1812	0.0436	2455	0.0009	0.0178	0.5456	0.5571	431.9	0.0054	0.0009	0.0125	0.9763	0.0567	0.0464	-0.0302	-0.1029	-4.103	0.0009	-0.0079	0.0025	0.0027
56	30.27	-0.1324	3147	3.229	30.02	105.2	78.48	^******	23.65	2.182	0.009	17.91	2.219	0.2108	-0.0215	-0.1069	77.86	0.4055	-0.0278	0.289	0.2616

57	41.23	0.0319	3132	3.591	35.53	190.7	96.91	473.9	24.56	1.528	0.0105	48.95	3.51	0.151	-0.0252	-0.1275	45.15	0.5238	-0.0284	0.3983	0.2803
58	30.64	0.1083	3394	1.623	50.26	48.63	21.53	^****	8.784	0.2644	0.0232	16.67	2.791	0.1499	-0.0316	-0.1162	53.19	0.3071	-0.0139	0.178	0.1291
59	47.96	0.0108	2998	2.895	36.15	123.9	73.14	446.7	18.22	1.945	0.013	34.75	3.372	0.1799	-0.0262	-0.1184	68.14	0.4201	-0.0215	0.3118	0.2177
60	40.49	0.0673	3299	1.226	39.53	44.91	29.73	455.6	10.25	0.3271	0.0192	16.42	3.204	0.2257	-0.0318	-0.1138	100.8	0.2654	-0.0142	0.1572	0.1141
61	35.11	0.039	2660	2.105	47.94	81.32	31.68	^****	12.07	0.8699	0.0154	15.33	3.632	0.1604	-0.023	-0.0966	62.83	0.2874	-0.0147	0.1621	0.2132
62	73.77	0.0518	2697	2.627	24.35	153	87.85	424.5	16.96	1.29	0.0113	40.19	4.139	0.4476	-0.0251	-0.1224	171.4	0.3661	-0.0284	0.3237	0.2369

63	0.1381	-0.0029	3034	0.0009	0.0384	0.418	0.4471	448.4	0.0093	0.0012	0.0099	4.199	0.0447	0.042	-0.0323	-0.0969	-5.426	0.001	-0.0085	-0.0007	0.004
64	59.34	-0.0164	2898	1.823	37.55	78.65	72.99	441.6	19.73	0.358	0.0189	15.81	4.978	0.2026	-0.028	-0.1085	82.86	0.3737	-0.021	0.2957	0.1783
65	35.75	0.1448	3021	1.629	51.63	82.65	17.89	465.7	8.101	0.2836	0.0252	12.19	2.895	0.1132	-0.026	-0.1083	33.91	0.2975	-0.0157	0.2728	0.2445
66	68.14	0.0386	2675	2.894	25.1	173.8	98.57	419.1	19.39	2.751	0.0109	42.92	4.346	0.2856	-0.0243	-0.1206	122.66	0.4066	-0.0268	0.3636	0.2679
67	76.82	0.0297	2487	2.437	14.98	80.83	78.43	424.5	11.52	0.9512	0.0113	35.87	2.918	0.3678	-0.0293	-0.1095	134	0.2754	-0.0201	0.2077	0.1625
68	43.56	0.0445	2935	1.92	49.66	57.35	23.45	438.2	9.723	0.4674	0.0165	19.03	4.527	0.1747	-0.0274	-0.1037	72.59	0.2756	-0.013	0.1084	0.187

69	62.35	0.3251	2829	2.737	26.14	262	92.48	435.8	19.17	2.783	0.0116	44.59	4.852	0.2804	-0.0224	-0.1374	118.1	0.4183	-0.0303	0.335	0.2778
70	73.79	0.0252	2512	2.337	33.88	79.44	51.89	430.4	14.69	0.6168	0.0168	10.43	4.203	0.2647	-0.0282	-0.1101	100.4	0.218	-0.0198	0.2343	0.2526
73	41.32	-0.0428	3114	1.473	6.861	51.79	74.6	458.2	9.201	0.188	0.0108	40.13	1.134	0.1674	-0.0316	-0.1075	58.39	0.2345	-0.0172	0.1692	0.0832
75 - 50 microns	18.63	0.0303	3.901	1.626	22.87	11.38	1.031	0.9796	3.296	0.156	0.0014	7.765	0.4497	0.0166	0.0022	-0.0031	3.297	0.1044	-0.001	0.0252	0.0374
75 - filtered	3.072	0.0179	6.399	0.1375	4.717	0.9338	0.8308	1.121	0.9715	0.0244	0.0023	8.239	0.1043	0.0082	0.0017	0	3.571	0.0231	0.0001	0.0039	0.0112
79 - 50 microns	23.28	0.0274	3.151	2.371	34.4	14.99	1.185	0.9302	4.903	0.2474	0.0011	8.45	0.6625	0.0188	0.0035	-0.0026	3.74	0.1633	-0.002	0.0397	0.0619
79 - filtered	4.458	0.026	3.612	0.3558	9.046	2.114	0.7821	0.8292	1.566	0.0554	0.0021	8.441	0.1226	0.0088	0.0032	-0.0019	3.437	0.0466	0.0004	0.0077	0.0149

80	56.61	0.0393	2839	2.958	24.2	106.9	96.1	440.1	22.06	0.4201	0.0107	30.58	2.64	0.1907	-0.0258	-0.1097	75.68	0.2981	-0.022	0.3204	0.2101
81	81.29	0.0959	2434	2.576	23.85	108.1	90.08	428.8	15.5	2.516	0.0139	38.04	6.584	0.3523	-0.0281	-0.1279	113.7	0.368	-0.0254	0.2829	0.266
82	82.4	0.04	2556	2.432	32.06	107.5	96.94	435.8	25.84	0.4426	0.0141	8.611	4.032	0.1963	-0.0267	-0.1252	66.86	0.239	-0.0231	0.338	0.3774
83	36.33	0.0511	3134	1.54	42.37	48.32	23.66	464.3	10.01	0.2953	0.0175	17.36	2.907	0.1181	-0.0296	-0.1056	37.92	0.243	-0.0145	0.121	0.0887
84	41.52	-0.0127	3065	2.217	34.65	76.21	62.1	460.3	16.81	1.775	0.0166	25.55	10.51	0.2872	-0.0255	-0.1083	118.2	0.3781	-0.0193	0.2478	0.3765
85 - 50 microns	24.72	0.0408	2.529	3.995	44.28	22.54	1.911	0.8143	7.326	0.2678	0.0011	6.512	0.7256	0.0173	0.0033	-0.003	3.966	0.2112	-0.0023	0.0319	0.0456

85 - filtered bottom	8.105	0.0282	3.414	0.685	11	3.676	1.022	0.7561	2.006	0.0621	0.0027	7.585	0.1542	0.01	0.0021	-0.001	3.051	0.057	-0.0006	0.0077	0.0271
87	48.62	0.0229	3018	2.859	36.71	121.3	73.02	445.6	19.2	1.738	0.0134	36.73	3.881	0.2463	-0.028	-0.1166	107.1	0.419	-0.0232	0.3237	0.2221
89 - 50 microns	13.06	0.0293	2.758	1.339	17.08	7.036	0.8707	0.8747	2.608	0.109	0.0015	5.569	0.2739	0.0108	0.0017	-0.0022	2.332	0.0789	-0.0002	0.0211	0.0183
89 - filtered	4.314	0.018	4.491	0.1871	4.85	1.491	0.7391	0.8851	0.8849	0.0275	0.0025	6.261	0.1624	0.0064	0.0022	0.0001	2.982	0.0227	-0.0002	0.0045	0.0173
90	27.12	-0.0112	3143	2.649	33.94	109.5	54.7	*******	17.76	1.431	0.012	12.99	2.918	0.2477	-0.021	-0.1048	98.25	0.3325	-0.0285	0.319	0.2334
91	29.68	0.0051	3148	1.42	44.4	35.99	28.56	*******	12.01	0.2266	0.0161	7.394	3.29	0.1286	-0.0234	-0.0999	41.77	0.2703	-0.0203	0.1866	0.1397

92	78.43	-0.0158	1366	1.198	5.995	74.25	83.32	325.1	8.537	0.4687	0.0067	41.01	1.409	0.1538	-0.0145	-0.0689	54.66	0.2146	-0.0196	0.1755	0.1006
93	28.02	0.0244	3109	1.921	54.17	40.57	17.53	^**** *	10.34	0.8236	0.0156	7.567	2.589	0.1126	-0.0239	-0.1019	34.03	0.2527	-0.0183	0.1192	0.1809
94	72.95	0.0535	2309	1.623	45.26	39.95	40.01	419.6	10.91	0.2931	0.0212	15.74	5.293	0.1525	-0.0302	-0.1106	40.83	0.301	-0.0169	0.1658	0.2409
95	80.73	0.0308	2284	3.023	39.36	88.79	63.92	418.2	18.29	0.4717	0.016	8.055	4.932	0.185	-0.0266	-0.1178	55.2	0.2483	-0.0226	0.2644	0.2126
96	81.91	0.0165	2355	2.993	27.3	118.3	104	424	19.28	0.8505	0.0107	48.34	4.061	0.4911	-0.0268	-0.1176	175.3	0.4365	-0.0288	0.2977	0.2613
44	31.51	0.0632	3095	1.637	39.59	51.68	30.29	^**** *	12.33	0.2807	0.0198	15.03	2.887	0.1855	-0.0275	-0.1039	75.27	0.2574	-0.0138	0.176	0.1468

72	78.53	0.0825	2285	1.429	34.31	46.78	44.72	423	11.7	0.2055	0.022	11.85	4.585	0.112	-0.0307	-0.1064	24.42	0.2438	-0.0152	0.1838	0.145
72 - 65082	83.23	-0.0253	2178	4.062	40.66	60.05	53.88	437.6	15.57	0.2206	0.0128	31.63	5.681	0.3905	-0.0265	-0.1076	131.7	0.4311	-0.0231	0.2773	0.1855

Appendix V

Magnetic Susceptibility Data

Depth (contiguous cm)	SI
1	1
2	1
3	1
4	1
5	1
6	1
7	2
8	2
9	2
10	4
11	4
12	5
13	7
14	7
15	8
16	9
17	9
18	9
19	9
20	9
21	9
22	10
23	9
24	10

25	10
26	9
27	8
28	8
29	7
30	6
31	7
32	6
33	6
34	6
35	6
36	6
37	6
38	7
39	7
40	7
41	7
42	7
43	6
44	6
45	7
46	5
47	5
48	4
49	2
50	2
51	1
52	0

57	1
58	2
59	3
60	3
61	5
62	6
63	6
64	5
65	5
66	4
67	5
68	5
69	6
70	6
71	5
72	3
73	2
74	2
75	1
76	1
77	1
78	1
79	1
80	1
81	1
82	1
83	0
84	0

85	1
86	0
87	1
88	1
89	1
90	1
91	0
92	1
93	1
94	1
95	1
96	1
97	0
98	0
99	1
100	0
101	1
102	0
103	0
104	0
105	0
106	0
107	0
108	0
109	0
110	0
111	0
112	0

113	0
114	-1
115	0
116	0
117	-1
122	-1
123	0
124	0
125	0
126	1
127	1
128	2
129	2
130	2
131	1
132	1
133	2
134	2
135	2
136	3
137	3
138	2
139	1
140	1
141	0
142	0
143	0
144	0

145	0
146	0
147	0
148	0
149	0
150	0
151	0
152	0
153	0
154	0
155	-1
156	-1
157	0
158	0
159	-1
160	0
161	-1
162	0
163	0
164	-1
165	0
166	0
167	0
168	0
173	1
174	2
175	2
176	2

177	2
178	2
179	2
180	1
181	1
182	0
183	0
184	0
185	0
186	0
187	0
188	0
189	0
190	0
191	0
192	0
193	-1
194	-1
195	0
196	-1
197	0
198	0
199	-1
200	0
201	-1
202	0
203	0
204	-1

205	0
206	0
207	-1
208	-1
209	0
210	-1
211	0
212	0
213	-1
214	0
215	0
216	0
217	-1
218	0
219	0
220	0
221	0
222	-1
223	0
224	0
225	0
226	0
227	0
228	0
233	0
234	1
235	1
236	1

237	1
238	1
239	0
240	0
241	0
242	0
243	-1
244	0
245	0
246	-1
247	-1
248	-2
249	-2
250	-1
251	-2
252	-1
253	-2
254	-1
255	-2
256	-1
257	-1
258	-2
259	-2
260	-2
261	-2
262	-1
263	-1
264	-1

265	-1
266	-2
267	-2
268	-1
269	-2
270	-2
271	-2
272	-2
273	-1
274	-2
275	-1
276	-1
277	-2
278	-1
279	-1
280	-2
281	-2
282	-2
287	1
288	2
289	2
290	3
291	3
292	4
293	3
294	4
295	3
296	3

297	3
298	2
299	1
300	1
301	1
302	1
303	0
304	0
305	0
306	0
307	1
308	0
309	1
310	0
311	1
312	1
313	1
314	0
315	-1
316	-1
317	0
318	-1
319	0
320	0
321	0
322	-1
323	-1
324	0

325	0
326	0
327	0
328	0
329	0
330	0
331	0
332	0
333	0
334	-1
335	-1
336	0
337	0
338	-1
343	1
344	2
345	1
346	1
347	1
348	2
349	1
350	2
351	1
352	2
353	1
354	1
355	0
356	0

357	0
358	0
359	0
360	0
361	0
362	0
363	0
364	0
365	0
366	0
367	0
368	0
369	1
370	4
371	8
372	14
373	15
374	13
375	7
376	3
377	2
378	1
379	0
380	0
381	0
382	0
383	0
384	0

385	-1
386	0
387	0
388	-1
389	-1
390	0
391	0
392	0
393	0
398	-1
399	-1
400	-1
401	0
402	1
403	1
404	2
405	2
406	3
407	2
408	2
409	2
410	2
411	1
412	1
413	0
414	-1
415	-1
416	-1

417	0
418	0
419	0
420	0
421	-1
422	0
423	0
424	0
425	-1
426	-1
427	-1
428	0
429	0
430	-1
431	-1
432	0
433	-1
434	-1
435	-1
436	0
437	-1
438	-1
439	-1
440	-1
441	0
442	0
443	0
444	1

445	1
446	1
447	2
448	2
449	2
450	2
451	3
452	2
453	2
454	2
455	1

Appendix VI

^{14}C Age Data

Sample ID	UGAMS #	pmC	±	1 s	Radiocarbon Age (YBP)			d13C corrected Radiocarbon Age (YBP)			Activity dpm/gmC			d13C corrected Activity dpm/gmC		d13C corrected Activity ERR dpm/gmC	d13C
David Tingey BYU recd 02/29/2016 INV#17075 Randy has separate splits for delta 13C																	
UMC-1 1:27	A24174	111.06	±	0.34	modern			modern			15.0593	±	0.0457	15.0730	±	0.0457	-25.9
UMC-1 2:16	A24175	**NO AMS**															-30.1

UMC-1 3:32	A24176	57.92	±	0.21	4387	±	29	4368	±	29	7.8541	±	0.0287	7.8720	±	0.0288	-27.3
UMC-1 4:32	A24177	49.01	±	0.18	5728	±	29	5696	±	29	6.6460	±	0.0240	6.6731	±	0.0241	-29.1
UMC-1 5:41	A24178	39.71	±	0.16	7419	±	31	7396	±	31	5.3845	±	0.0210	5.4003	±	0.0211	-27.9
UMC-1 6:40	A24179	34.72	±	0.15	8497	±	33	8462	±	33	4.7083	±	0.0197	4.7290	±	0.0197	-29.4
UMC-1 7:42	A24180	38.64	±	0.15	7639	±	31	7595	±	31	5.2392	±	0.0207	5.2683	±	0.0209	-30.6
UMC-1 8:58.5	A24181	30.08	±	0.13	9650	±	35	9634	±	35	4.0788	±	0.0179	4.0873	±	0.0179	-27.1
11978	A24182	**NO AMS**															-9.5
11979	A24183	**NO AMS**															-9.7
FIRI D,F	Af022416b	57.19	±	0.20	4489	±	28	4489	±	28	7.7547	±	0.0275	7.7547	±	0.0275	-25
CAIS anthracite	B00_7022	0.094	±	0.005	55961	±	462	55961	±	462	0.0128	±	0.0007	0.0128	±	0.0007	-25
David Tingey BYU recd 02/29/2016																	

INV#17076 Randy has separate splits for delta 13C																	
12351	A24184				#DIV/0!			#DIV/0!	±		0.0000	±	0.0000	0.0000	±	0.0000	-10.9
12357	A24185				#DIV/0!			#DIV/0!	±		0.0000	±	0.0000	0.0000	±	0.0000	-3.8
12362	A24186				#DIV/0!			#DIV/0!	±		0.0000	±	0.0000	0.0000	±	0.0000	-6.7
12370	A24187				#DIV/0!			#DIV/0!	±		0.0000	±	0.0000	0.0000	±	0.0000	-5.9
12371	A24188				#DIV/0!			#DIV/0!	±		0.0000	±	0.0000	0.0000	±	0.0000	-5.0
12378	A24189				#DIV/0!			#DIV/0!	±		0.0000	±	0.0000	0.0000	±	0.0000	-8.2
12379	A24190				#DIV/0!			#DIV/0!	±		0.0000	±	0.0000	0.0000	±	0.0000	-7.1

Appendix VII

Pyrolysis Data

Sample ID	Age (BP)	Contiguous Depth (cm)	Weight (mg)	S1-Free Oil (mgHC/g rock)	S2-Kerogen Yield (mgHC/g rock)	S3 (mgCO2/g rock)	Tmax-Maturity (°C)	TOC-Total Organic Carbon (Weight %)	CC-Carbonate Carbon (Weight %)	GOC-Generative OC (Weight %)	NGOC-Non-generative OC (Weight %)	AI-Adsorption Index (Weight %)	OSI-Oil Sat.Index (mgHC/gTOC)	PI-Production Index	HI-Hydrogen Index (mgHC/gTOC)	OI-Oxygen Index (mgCO2/gTOC)
UMC-1 1:9	0	1	19.9	0.35	54.42	7.8	287	12.13	0.36	4.94	7.19	9.95	2	0	448	64
UMC-1 1:14	0	6	21.5	0.27	49.09	8.49	286	11.7	0.27	4.48	7.21	9.59	2	0	419	72
UMC-1 1:20	0	12	20.5	0.2	5.48	2.24	427	3.2	0.26	0.56	2.64	2.63	6	0.04	171	69
UMC-1 1:26	0	18	19.1	0.21	1.96	1.7	420	1.94	0.27	0.27	1.67	1.59	10	0.1	101	87
UMC-1 1:32	841	24	24.1	0.16	1.44	2.21	420	1.7	0.25	0.21	1.49	1.4	9	0.1	84	130

UMC-1 1:38	1051	30	21.4	0.19	1.83	1.9	421	1.93	0.16	0.25	1.68	1.59	9	0.09	94	98
UMC-1 1:44	1261	36	26.5	0.15	3.53	1.95	430	2.89	0.18	0.39	2.5	2.37	5	0.04	121	67
UMC-1 1:50	1471	42	22.4	0.18	1.98	2.84	427	2.18	0.18	0.28	1.9	1.79	8	0.08	90	130
UMC-1 1:56	1681	48	20.6	0.19	3.53	2.4	431	3.12	0.39	0.42	2.7	2.56	6	0.05	113	77
UMC-1 2:3	2067	59	20.6	0.22	37.04	5.21	437	8.78	0.31	3.35	5.43	7.2	2	0	421	59
UMC-1 2:9	2277	65	20.9	0.19	2.1	2.62	430	2.41	0.19	0.3	2.12	1.98	7	0.08	86	108
UMC-1 2:15	2487	71	24.1	0.19	21.14	3.76	437	6.79	0.37	1.95	4.84	5.57	2	0	311	55
UMC-1 2:21	2702	77	21.9	0.2	24.93	5.28	437	9.28	0.35	2.32	6.95	7.61	2	0	268	56
UMC-1 2:27	2919	83	19.5	0.26	42	5.26	437	9.36	0.27	3.79	5.57	7.67	2	0	448	56

UMC-1 2:33	3136	89	22.3	0.19	6.94	2.04	428	3.98	0.18	0.69	3.29	3.26	4	0.03	174	51
UMC-1 2:39	3353	95	22.1	0.32	58.96	6.69	435	12.48	0.3	5.29	7.19	10.24	2	0	472	53
UMC-1 2:45	3570	101	22.1	0.44	75.19	10	433	16.01	0.36	6.78	9.23	13.13	2	0	469	62
UMC-1 2:51	3787	107	19.3	0.48	82.65	10.19	431	18.1	0.38	7.43	10.66	14.84	2	0	456	56
UMC-1 2:57	4004	113	21.3	1.17	131.39	17.49	427	29.12	0.53	11.87	17.25	23.88	4	0	451	60
UMC-1 3:18	4403	124	22.5	0.49	59.96	9.34	420	14.87	0.32	5.47	9.39	12.19	3	0	403	62
UMC-1 3:24	4620	130	24	0.17	12.5	3.61	432	5.11	0.27	1.21	3.91	4.19	3	0.01	244	70
UMC-1 3:30	4837	136	22.4	0.18	4.82	2.71	430	3.41	0.25	0.53	2.88	2.8	5	0.04	141	79
UMC-1 3:36	5023	142	19	0.94	98.16	16.87	323	28.52	0.51	9.02	19.49	23.38	3	0.01	344	59

UMC-1 3:42	5178	148	22.6	0.56	88.06	10.12	328	20.3	0.29	7.91	12.39	16.64	2	0	433	49
UMC-1 3:48	5333	154	20.9	0.85	119.73	13.91	328	25.7	0.39	10.76	14.94	21.07	3	0	465	54
UMC-1 3:54	5489	160	20.3	0.7	132.89	12.97	332	28.29	0.37	11.83	16.45	23.19	2	0	469	45
UMC-1 4:6	5825	173	22.4	0.19	17.56	4.31	428	6.01	0.26	1.66	4.35	4.93	3	0.01	292	71
UMC-1 4:12	5980	179	22.2	0.19	9.2	2.76	434	4.49	0.29	0.9	3.59	3.68	4	0.02	204	61
UMC-1 4:18	6136	185	20.4	0.59	98.67	9.45	330	19.18	0.35	8.79	10.39	15.73	3	0	514	49
UMC-1 4:24	6291	191	20.3	0.67	141.6	12.39	332	29.21	0.36	12.54	16.68	23.95	2	0	484	42
UMC-1 4:30	6446	197	21.4	0.48	92.05	9.5	336	19.49	0.37	8.21	11.28	15.98	2	0	472	48
UMC-1 4:36	6606	203	19.4	0.66	128.13	11.97	335	26.01	0.41	11.39	14.62	21.33	2	0	492	46

UMC-1 4:41	6744	208	21.2	0.78	138.79	11.81	336	26.49	0.36	12.27	14.21	21.72	2	0	523	44
UMC-1 4:47	6908	214	22.9	0.67	149.66	14.65	335	27.73	0.47	13.29	14.44	22.74	2	0	539	52
UMC-1 4:53	7073	220	24.2	0.69	147.32	12.58	336	26.5	0.33	13.03	13.47	21.73	2	0	555	47
UMC-1 4:59	7238	226	22.2	0.57	104.3	10.02	332	18.52	0.3	9.27	9.25	15.19	3	0	563	54
UMC-1 5:16	7540	237	21.6	0.21	31.24	5.67	429	8.89	0.29	2.87	6.02	7.29	2	0	351	63
UMC-1 5:22	7705	243	22.7	0.53	107.39	10.33	335	21.02	0.33	9.55	11.47	17.24	2	0	510	49
UMC-1 5:29	7898	250	19.6	0.62	135.13	14.02	333	27.56	0.41	12.03	15.54	22.6	2	0	490	50
UMC-1 5:35	8063	256	19.6	0.74	152.49	13.12	335	25.84	0.42	13.49	12.35	21.19	2	0	590	50
UMC-1 5:41	8228	262	20.8	0.66	142.62	14.18	333	27.75	0.43	12.7	15.05	22.75	2	0	513	51

UMC-1 5:47	8369	268	23.5	0.7	170.31	14.95	336	35.81	0.39	15.06	20.75	29.36	1	0	475	41
UMC-1 5:53	8505	274	21.9	0.53	123.23	14.45	332	26.42	0.36	11.03	15.39	21.67	2	0	466	54
UMC-1 5:59	8641	280	21.2	0.58	123.8	16.33	330	27.31	0.37	11.13	16.18	22.39	2	0	453	59
UMC-1 6:13	8868	290	25.3	0.18	2.94	2.39	426	2.51	0.26	0.34	2.16	2.06	7	0.06	117	95
UMC-1 6:19	9005	296	23.2	0.2	26.45	4.45	324	8.63	0.29	2.43	6.2	7.08	2	0	306	51
UMC-1 6:25	9141	302	21.8	0.25	53.68	7.58	332	12.9	0.24	4.86	8.04	10.58	1	0	416	58
UMC-1 6:31	9277	308	21.8	0.24	46.75	6.09	329	11.34	0.27	4.22	7.12	9.3	2	0	412	53
UMC-1 6:37	9414	314	21.9	0.58	124.9	13.47	334	27.88	0.39	11.14	16.74	22.86	2	0	447	48
UMC-1 6:43	9526	320	21.1	0.52	111.88	13.51	331	23.5	0.35	10.03	13.47	19.27	2	0	476	57

UMC-1 6:49	9592	326	21.7	0.49	107.77	13.77	331	27.09	0.37	9.7	17.4	22.22	1	0	397	50
UMC-1 6:55	9659	332	20.3	0.48	89.43	11.03	332	22.39	0.41	8.03	14.36	18.36	2	0	399	49
UMC-1 6:61	9781	343	19.3	0.56	95.98	11.5	330	20.85	0.34	8.62	12.23	17.1	2	0	460	55
UMC-1 7:16	9837	348	22.8	0.19	3.89	2.46	427	3.04	0.27	0.43	2.61	2.49	6	0.05	127	80
UMC-1 7:22	9903	354	24.1	0.18	11.89	3.02	432	4.89	0.18	1.14	3.75	4.01	3	0.01	243	61
UMC-1 7:28	9970	360	20.9	0.28	49.78	6.56	330	11.64	0.23	4.49	7.15	9.55	2	0	427	56
UMC-1 7:34	10037	366	20.9	0.29	52.03	6.93	330	12.51	0.3	4.7	7.81	10.26	2	0	415	55
UMC-1 7:40	10103	372	24.5	0.32	61.04	7.7	330	14.88	0.27	5.49	9.39	12.2	2	0	410	51
UMC-1 7:46	10170	378	19	0.28	48.12	6.49	422	12.9	0.35	4.36	8.54	10.58	2	0	372	50

UMC-1 7:52	10237	384	19	0.28	48.97	7.98	327	14.67	0.29	4.49	10.18	12.03	1	0	333	54
UMC-1 7:58	10303	390	21.1	0.23	40.74	6.37	425	11.05	0.28	3.72	7.33	9.06	2	0	368	57
UMC-1 8:6	10426	401	22.2	0.23	39.06	7.24	426	11.83	0.32	3.59	8.23	9.7	1	0	330	61
UMC-1 8:12	10492	407	23.4	0.18	2.55	2.22	431	2.48	0.31	0.31	2.17	2.04	7	0.07	102	89
UMC-1 8:18	10559	413	21.5	0.22	26.19	4.61	428	8.11	0.33	2.41	5.69	6.65	2	0	323	56
UMC-1 8:24	10626	419	20.8	0.27	38.61	5.91	329	10.25	0.25	3.52	6.73	8.4	2	0	376	57
UMC-1 8:30	10692	425	19.7	0.36	67.87	8.74	330	16.46	0.3	6.12	10.34	13.5	2	0	412	53
UMC-1 8:36	10759	431	24.7	0.24	63	8.92	330	16.13	0.28	5.71	10.42	13.23	1	0	390	55
UMC-1 8:42	10826	437	21.4	0.23	40.36	6.91	420	12.4	0.27	3.71	8.69	10.17	1	0	325	55

UMC-1 8:48	10892	443	23.8	0.18	9.5	3.42	423	5.65	0.21	0.95	4.7	4.63	3	0.02	168	60
UMC-1 8:54	10959	449	20.4	0.2	2.17	1.42	412	1.74	0.22	0.26	1.48	1.43	11	0.08	124	81
UMC-1 8:60	11027	455	21.6	0.19	1.6	0.89	414	1.38	0.22	0.2	1.18	1.13	13	0.11	116	64

Appendix VIII

Core Log Notes and Description

	Word	Percentage					
	Dominant	>50%					
	Abundant	25-50%					
	Common	5-25%					
	Trace	<1%					
Drive	Beginning Depth (cm)	Ending Depth (cm)	Color (Munsell)	Color Number	Macroscopic Description	Microscopic Description	Interpretation
1	0	9	N/A				N/A

1	9	20	Dusky yellowish brown	10 YR 2/2	mostly rootlets with clay	Abundant diatoms 50% organic, 50% clastic. Clastic 50% clay, 30% silt, 20% sand	Organic rich, silty clay with abundant diatoms. Interval dominated by rootlets.
1	20	57	Pale brown	5 YR 5/2	with lots of dark yellowish orange (10 YR 6/6) laminations	Trace diatoms and pollen with aquatic amorphous organic matter and aquatic vascular organic matter. 70% silt 25% clay 5% sand. 30% biogenic	Laminated clayey silt with trace diatoms and abundant organic matter
1	57	58	Olive black	5 Y 2/1	organic fragments 1 mm long (<10%)	50% clay, 50 % silt; 80% biogenic with abundant diatoms, abundant plant cells, and rare pollen	Silty clay (50/50) dominated by biogenic matter with rare organic fragments about 1 mm long; with abundant diatoms, abundant plant cells, and rare pollen.
1	58	61	N/A				N/A
2	0	4.5	Olive black (Same as above)			50% clay, 50 % silt; 80% biogenic with abundant diatoms, abundant plant cells, and rare pollen	Silty clay (50/50) dominated by biogenic matter with rare organic fragments about 1 mm long; with abundant diatoms, abundant plant cells, and rare pollen.

2	4.5	14	Grayish brown	5 YR 3/2	mud	60% clastic, 40% biogenic. Plant cells common, trace diatoms, common carbonized soil organic matter	Silty clay (50/50) with abundant biogenic matter. Plant cells and carbonized soil organic matter common, with trace diatoms.
2	14	37	Dark yellowish brown	10 YR 4/2	Clay. Prolific laminations of live black (5 Y 2/1), rare 1 - 5 mm long organic fragments	30% clastic, 70% biogenic; abundant diatoms (80%), terrestrial organic matter including rare pollen and carbonized soil organic matter	Silty clay (50/50) dominated by diatoms with rare organic fragments 1-5 mm. Organic matter common with rare pollen and rare carbonized soil organic matter.
2	37	53	Dark yellowish brown	10 YR 4/2	Clay. Prolific laminations of live black (5 Y 2/1), common 1 -5 mm organic fragments	50% clastic, 50% biogenic with abundant diatoms and common pollen and terrestrial plant matter	Silty clay (50/50) with abundant diatoms with common organic fragments 1-5 mm. Organic matter common with common pollen and rare carbonized soil organic matter.
2	53	61	Grayish black	N 2	Peat. Abundant organic fragments <7mm, less consolidated	10% clastic, 90% biogenic. 50% organic matter, 40% siliceous matter	Peat with rare pollen
3	0	14.5	N/A				N/A

3	14.5	18.5	Grayish black	N 2	Peat	Peat with clay common	Peat with clay common
3	18.5	31	Moderate yellowish brown	10 YR 5/4	Clump of 2.5 cm x 4 cm olive black 5 Y 2/1 clay	Biogenically dominated clay with abundant diatoms and rare pollen	Biogenically dominated silty clay with abundant diatoms and rare pollen
3	31	61	Grayish black	N 2	Clumpy, less consolidated peat	Silty clay with abundant biogenic matter	Peaty, silty, poorly consolidated clay with abundant biogenic matter, including plant fragments ranging from 10 - 1500 micrometers
4	0	6	N/A				N/A
4	6	10	dark yellowish brown	10 YR 4/2	mostly rootlets with clay	Sandy silt with abundant biogenic matter and diatoms	Organic rich, silty clay with abundant diatoms and dominated by rootlets. Most likely some surface sediment dropped down hole while coring
4	10	12	Dusky yellowish brown	10 YR 2/2	clay	Silty clay with abundant organic and siliceous biogenic matter	Clayey silt with abundant organic and siliceous biogenic matter

4	12	61	Grayish black	N 2	Peat	Peat with rare pollen and abundant silt	Peat with rare pollen and abundant silt
5	0	11	N/A				
5	11	14	Dusky yellowish brown	10 YR 2/2	Well consolidated clay	Sandy, silty clay with abundant biogenic components including rare pollen and common diatoms	Sandy, silty clay with abundant biogenic components including rare pollen and common diatoms
5	14	60	Grayish black	N 2	Peat with abundant clay	Peat with abundant clay	Peat with abundant clay
5	60	61	N/A				
6	0	9	N/A				
6	9	20	Dark yellowish brown	10 YR 4/2	Clay	Silty clay with common biogenic components including rare diatoms	Silty clay with common biogenic components including rare diatoms
6	20	26	brownish black	5 YR 2/1	Peat	Large plant matter - 1400 micrometers. Silty clay dominated by biogenic components with dominant organic matter and common diatoms and trace pollen	Peat with diatoms common and abundant silty clay

6	26	35	Brownish black	5 YR 2/1	3cm x 2cm clump of dark yellowish brown (10 YR 4/2) clay in clayey peat. Peat more consolidated than that uphole. Some light brown 5 YR 5/6 precipitate in pores of lower 2cm	Clayey silt with abundant biogenic components, common diatoms and trace pollen	Peat with clayey silt, common diatoms, and trace pollen
6	35	61	Grayish black	N 2	less consolidated peat	Peat with dominant organic matter and common silt	Peat with dominant organic matter and common silt
7	0	10	N/A				
7	10	24	Dark yellowish brown	10 YR 3/2	finely laminated clay	Clay with common biogenic matter containing common diatoms	Finely laminated clay with rare diatoms
7	24	35	Dusky yellowish brown	10 YR 2/2	fine organic fragment matrix with silty peat of medium consolidation	Silt with abundant biogenic components including common diatoms and rare pollen	Medium consolidated peat with common diatoms and rare pollen, dominated by silt
7	35	61	Olive black	5 Y 2/1	Organic fragment moderately rich matrix of medium consolidation with vuggy porosity displaying light brown (5 YR 5/6) precipitates	Peat with abundant clay	Poorly consolidated peat with abundant clay and vuggy porosity lined with brown precipitate

					in between and a wood chip 1.5cm x 1cm		
8	0	2	N/A				
8	2	9	Dusky yellowish brown	10 YR 2/2	organic rich clay, vuggy porosity, and medium consolidation	Clay with common biogenic components including trace diatoms and trace pollen	Clay with common biogenic components including trace diatoms and trace pollen
8	9	17	Moderate yellowish brown	10 YR 5/4	Areas of medium gray N 5 clay	Clay with common biogenic components	Clay with common biogenic components
8	17	31	Dusky yellowish brown	10 YR 2/2	Medium high consolidation, vuggy, organic rich clay	Clay with abundant biogenic components including common diatoms and plant matter with organic matter blobs	Clay with abundant biogenic components including common diatoms and organic matter
8	31	35	Dark yellowish brown	10 YR 4/2	well consolidated clay with organic fragments	Clayey silt with abundant biogenic components, primarily diatoms	Clayey silt with organics fragments, and abundant biogenic components, primarily diatoms

8	35	39	Dusky yellowish brown	10 YR 2/2	clay with organic fragments	Clayey silt dominated by biogenic components including common diatoms, dominated by organic matter	Clayey silt dominated by organic matter with common diatoms
8	39	40.5	Dark yellowish brown	10 YR 4/2	clay with organic fragments	Clayey, silty, peat with abundant diatoms	Clayey silt dominated by organic matter with common diatoms
8	40.5	46	Dusky yellowish brown	10 YR 2/2	Vuggy organic rich silty peat	Peat with common silt, abundant diatoms, and common pollen	Peat with common silt, abundant diatoms, and common pollen
8	46	48.5	Olive black	5 Y 2/1	clay	Clay with common biogenic components	Clay with common biogenic components
8	48.5	53	Greenish black	5 GY 2/1	Clay	Sandy, silty clay with common organic matter and trace diatoms	Sandy, silty clay with common organic matter and trace diatoms
8	53	61	Moderate brown	5 YR 4/4	Sandy clay	Sandy, silty clay with abundant biogenic components including terrestrial plant matter	Sandy, silty clay with abundant biogenic components including terrestrial plant matter